



UNIVERSIDAD AUTÓNOMA DE SAN LUIS POTOSÍ

Facultad de Ciencias



Functionalization of Nanomaterials Based on Zero-Valent Iron for Water Treatment

Tesis

Para obtener el título de:
Maestro en Ciencias Aplicadas

Presenta:

Ing. Claudio Adrián Ruiz Torres

Asesor de tesis:

Dr. Gabriel Alejandro Martínez Castañón

Co-Asesor:

Dr. J. Elpidio Morales Sánchez

Co-Asesor:

Dr. Yuhoon Hwang

Functionalization of Nanomaterials Based on Zero-Valent Iron for Water Treatment

Tesis que presenta:

Ing. Claudio Adrián Ruiz Torres

A la comisión integrada por:

Dr. Gabriel Alejandro Martínez Castañón.

Asesor de tesis

Dr. J. Elpidio Morales Sánchez.

Co-Asesor

Dra. Nereyda Niño Martínez.
Sinodal

Dr. Salvador A. Palomares Sánchez
Sinodal

Dedicatoria

“A quien supo guiarme por el buen camino, darme fuerza para seguir adelante y no desmayar en los problemas que se presentaban, enseñándome a encarar las adversidades sin perder nunca la dignidad ni desfallecer en el intento”

Dios

A mis padres Facundo Ruiz y Ma. de los Ángeles Torres

Quienes me han dado amor, paciencia, apoyo y comprensión en todo momento

A mi abuela Clara Ruiz

Por su amor, consejos y sabiduría

A mis hermanos: David Israel, Brenda Izanami, Luis Ángel, Clara Adriana, y a mi novia Karen Sánchez

Por su apoyo total y motivación constante

GRACIAS

ACKNOWLEDGEMENTS

This work is supported by the National Research Foundation of Korea (NRF) grant funded by the Korea government (MSIP; Ministry of Science, ICT, & Future Planning) (No. NRF-2017R1C1B5015387).

Claudio Adrian Ruiz Torres would like to thank to Consejo Nacional de Ciencia y Tecnología (CONACYT) for its support with the scholarship No. 412287.

CONTENT

CHAPTER 1	6
1. INTRODUCTION	6
CHAPTER 2	9
Preparation of air stable nanoscale zero valent iron functionalized by ethylene glycol without inert condition	9
2. ABSTRACT	9
2.1 INTRODUCTION	10
2.2 MATERIALS AND METHODS	12
2.2.1 Synthesis and functionalization of nZVI	12
2.2.2 Physical characterization methods	13
2.2.3 Reactivity measurements	14
2.2.3.1 Reactive iron contents	14
2.2.3.2 Nitrate reduction capacity	14
2.3. RESULTS AND DISCUSSION	14
2.3.1 nZVI functionalization by ethylene glycol	14
2.3.1.1 Functionalization mechanism	14
2.3.2 Increased dispersibility by nZVI functionalization	17
2.3.3 Air stability of functionalized nZVI	18
2.3.3.1 Structural characterization - XRD	19
2.3.3.2 Morphological characterization – TEM and EDS	20
2.3.3.3 Effect of oxidation on nZVI reactivity	23
2.4 CONCLUSIONS	25
CHAPTER 3	26
Ultrasmall and high stable, size controlled nano zero valent iron preparation using non-aqueous solvent with functionalization agent	26
2. ABSTRACT	26
2.1 INTRODUCTION	27
2.2 MATERIALS AND METHODS	29
2.2.1 Reagents	29
2.2.2 nZVI synthesis	29
2.2.3 Physical characterization methods	30
2.2.4 Reactivity analysis	30
2.3 RESULTS AND DISCUSSION	30
2.3.1 Functionalized nZVI prepared by non-aqueous reduction	30
2.3.1.1 Stabilization mechanisms	30
2.3.1.2 Ultraviolet–visible (UV–Vis) absorption spectroscopy	32
2.3.1.3 Fourier transform infrared spectroscopy (FTIR)	33
2.3.2 Size control using non-aqueous solvent with stabilization agent	35
2.3.2.1 Morphological characterization – TEM	35

2.3.2.2	Size distribution analysis	35
2.3.2.3	Dynamic light scattering (DLS) and Zeta potential.....	39
2.3.2.4	Sedimentation analysis for nano-suspension stability examination	39
2.3.3	Effect of functionalization in reactivity of nZVI	41
2.3.3.1	X-Ray diffraction.....	41
2.3.3.2	Reactive iron content	43
2.3.3.3	Nitrate reduction	43
2.4	CONCLUSIONS	44
CHAPTER 4	45
3. CONCLUSIONS	45
REFERENCES	46

LIST OF FIGURES

Graphical abstract	6
Figure 1. A) UV–Vis aqueous absorption spectra of FeCl ₃ , [Fe(EG)] ³⁺ and spectra of nZVI functionalized with EG. B) FTIR spectrum of EG and nZVI-EG.....	12
Figure 2 Schematic illustration showing Fe ³⁺ coordination process and functionalization of nZVI by EG.....	13
Figure 3. A-B) TEM photomicrography of nZVI-EG and S-nZVI and their corresponding histograms. C) Schematic model of ZVI nanochains.....	14
Figure 4 Sedimentation curves of nZVI and nZVI-EG.....	15
Figure 5 Powder X-ray diffraction (XRD) patterns of nZVI and functionalized nZVI dried in anaerobic and aerobic conditions	17
Figure 6 A-B) TEM photomicrography of nZVI-EG ₂ and S-nZVI ₂	18
Figure 7 A-D) HR-TEM photomicrography of nZVI samples (A: nZVI-EG ₁ , B: nZVI-EG ₂ , C: S-nZVI ₁ , D: S-nZVI ₂). E-H) Energy dispersive spectrometer scanning line (EDS) of nanoparticles with and without functionalization dried in aerobic and anaerobic conditions (E: nZVI-EG ₁ , F: nZVI-EG ₂ , G: S-nZVI ₁ , H: S-nZVI ₂).	19
Figure 8. A) Reactive iron content of nZVI samples. B) Nitrate reduction by nZVI samples. C) Dissolved iron concentration during nitrate reduction.....	22
Figure 9. Schematic illustration showing: (A) Fe ³⁺ coordination process, functionalization of nZVI-EG _{non-aq} and size-control. (B) Fe ³⁺ coordination and uncontrolled grow of S-nZVI _{non-aq}	29
Figure 10. A) FeCl ₃ aqueous and non-aqueous spectrum. B) UV–Vis absorption spectra of H ₂ O:MEOH; 100-0, 75-25, 50-50, 25-75 and 0-100%. C) [Fe(CH ₃ OH) ₄] ₃ in the presence of EG and nZVI functionalized with EG spectra. D) FTIR spectrum of EG and nZVI-EG _{non-aq}	30
Figure 11. A-B) TEM photomicrography of nZVI-EG and S-nZVI correspondingly.....	32
Figure 12. Differential and cumulative size distribution of A) nZVI-EG _{non-aq} , B) S-nZVI _{non-aq} and C) nZVI-EG _{aq} . D) Cumulative size distribution of the samples.	34
Figure 13. Sedimentation curves of nZVI and nZVI-EG.....	38
Figure 14. XRD pattern of S-nZVI and nZVI-EG.....	40
Figure 15. A) Reactive iron content of nZVI samples. B) Nitrate reduction by nZVI samples.....	41

LIST OF TABLES

Table 1	Rietveld refinement of a sample zero-valent iron nanochain with and without EG.....	20
Table 2	Composition of EDS points in Figure 7 E-H, wt%.....	23
Table 3	Band positions (cm^{-1}) for EG and EG nZVI functionalized.....	34
Table 4	Size distribution statistical parameters of ZVI materials in nm.....	39
Table 5	Dynamic light scattering (DLS) and Zeta potential of nZVI _{non-aq} samples.....	39
Table 6	Rietveld refinement of a sample zero-valent iron nanoparticle.....	43

CHAPTER 1

1. INTRODUCTION

Nanotechnology science is defined as the discipline in which the material is handled in the scale (1-100 nm). The use of this technology has received considerable attention in recent years due to its potential applications in numerous research sectors. Furthermore, the alarming population growth, as well as industrial activities, have to lead to elevated concentrations of a wide range of contaminants in wastewater and groundwater [1]. For that reason persist the need to find new and more efficient technologies in the purification and treatment of water.

Environmental nanotechnology provides novel tools in remediation based on the synthesis and application of advanced materials that can be functionalized whereby it is optimized their environmental application, acting as contaminant immobilizer in the environment or promoting its degradation [2,3]. A special case is the use of zero-valent iron nanoparticles (nZVI), that general structure of this material consists essentially of a particle composed of a reactive iron Fe(0) nucleus, which is widely known to form an iron oxide thin layer of variable thickness around the particle called core-shell; this layer is established by interaction of the metal core with oxygen present in the surrounding environment, creating a passivation of the surface that can take different crystalline structures such as Wüstite (FeO), magnetite (Fe₃O₄), maghemite (γ -Fe₂O₃) or Goethite (α -FeOOH) [4–7]. The main function of this layer is to avoid the additional oxidation of the particle [8]. The principal interest in this kind of nanomaterial is because their high surface area, standard redox potential ($E_0 = -0.44$ V), allowing a high rate of reactivity with contaminants, by electron transfer during the oxidation of Fe⁰ to Fe²⁺ and eventually Fe³⁺, making it an efficient reducing agent and oxidizing agent [9,10] and specific affinity for toxic contaminants in aqueous systems [11]: such as chlorinated organic solvents, organochlorine pesticides, organic dyes [12–14], and metal ions: such as Pb (II), Cu (II), Ni (II) and Cr (VI) [15–19].

The chemical methodologies for the synthesis of nZVI represent the most common and used option. Emphasizing the methodology reported by [4] which consists of the chemical reduction of a ferric salt (FeCl₃) in aqueous phase, using as reducing agent NaBH₄. Notwithstanding, exist some limitations in the synthesis and management, reducing the actual application of nZVI in environmental engineering, owing to high material tendency to react in response to large surface area; as a result of this, such nanomaterials are usually unstable when exposed to the air because of the high oxygen sensitive reducing the usefulness of the material. Implying, firstly, the necessity of inert conditions to avoid this phenomenon, which means the increment of the synthesis cost, reducing the applicability of the nanomaterial as a cost-effect solution in water purification. Moreover, related to this fact, the airborne stability of the material means a significant factor in its synthesis and handling. For that reason, in last years there has been considerable research to develop synthesis methods for the production of zero-valent iron nanomaterials [3,20] looking modify the surface

properties of the material [12,21,22]. Subsequently, the modification of the surface of the particles by the presence of a protective polymer layer allows increasing the stability of the nanomaterial because prevents the reaction with oxygen present in the environmental, avoiding a high rate of nZVI corrosion in the particle, which greatly reduces its reactivity and applicability.

Nevertheless, exist another important limiting variable in the research and production of materials of this type, owing to the need to find materials with greater efficiency in its application persists, which is related to the dimensions and the uniformity of the diameters in these. On the other hand, these should be obtained through simple and economical synthesis methodologies to become a cost-effective solution in environmental remediation.

Furthermore, there are several reports based on nanomaterials of zero-valent iron with ultrasmall sizes and narrow size distribution (<3-8 nm) using different methodologies making use of a stabilizing agent of variable composition which intensifies the reduction and control of particle size [21,23–25]. Notwithstanding, the synthesis techniques mentioned above can be fully classified as extremely complex and expensive methodologies, which require highly controlled conditions, making it impossible to use nZVI ultrasmall and narrow size distributions a decontamination agent in water purification. So the chemical reduction of ferrous ions continues as the most viable option in nZVI synthesis. However, by this methodology is generally shown nanoparticles with diameters in the range of 10-100 nm, which average sizes of 50-70 nm and a broad particle size distribution, which prove to be characteristic of said synthesis methodology [4,16,26–30]. Even modifying the nanoparticles surface by the presence of stabilized agent the average of the obtained particles show a broad size distribution (± 2 -60 nm) [31,32].

In response to this, using non-aqueous solvents, more specifically alcohols, as a substitute, have demonstrated have various benefits during the synthesis of nanomaterials, due to the physical properties of the non-aqueous solvent generates the particle stabilization [33–36].

Supplementary, there are counterproductive effects in the use of alcohols as solvents that generates the particle agglomeration and growth [35,37], by cause of this fact, the Non-aqueous solvent methodologies were reported as good methods in nanoparticle size decrease, but it is not enough to obtain ultrasmall and size controlled nZVI.

According to the factors that hindering the management and obtaining of nZVI mentioned above, there is a need to find new and simpler methodologies for obtaining air stable and size controlled nanoscale ZVI materials, for its application in the removal of contaminants from water.

In relation to the first limitation of the nanomaterial management mentioned above, which is associated with the

corrosion stability of the reactive nucleus, in this work, the first part of the research is based on the functionalization of the particles using ethylene glycol (EG) as a coating agent, to provide air stability to synthesized zero-valent iron nanoparticles and to control their corrosion during synthesis and drying. The functionalization led to better applicability of the material due to the modification of its surface, increasing nanoparticle dispersibility in aqueous media. To corroborate the advantages involved in the functionalization of the material and the air stability associated with EG presence, nZVI were obtained in the presence and absence of the coating agent; simple (S-nZVI) and stabilized (nZVI-EG) nanoparticles were obtained. The synthesis of the nanomaterials was carried out by a method of chemical reduction of aqueous ferric salts, which were functionalized with ethylene glycol at room temperature without inert conditions.

Subsequently, the second part of the manuscript is related with the obtaining of size-controlled nZVI. Accordingly, it was proposed the implementation of two stabilization mechanisms associated non-aqueous solvent use and the addition of a polymeric functionalizing agent for the stabilization of the nanoparticles by the grafting of EG brushes on the surface of the particles and is expected that the two organic molecules, MeOH and EG, make interaction with nZVI, helping nZVI growth in a controlled manner.

This part of the research presents a cost-effective synthesis method of narrow size distribution <7.5% nZVI (1–9 nm) generated by non-aqueous chemical reduction method of ferric salts and functionalized with ethylene glycol at room temperature without inert conditions. Additionally, the synthesis of zero-valent iron nanoparticles without coated agent (S-nZVI) was realized to compare the occurred effects in the different materials associated to the absence and presence of the functionalization.

Corresponding to both different stages of the present investigation, it was identified the mechanism of stabilization and functionalization present in each methodology. It was carried out the characterization of the materials in terms of crystallinity, morphology and colloidal stability, with the aim of identifying the changes associated with the stabilization and modification of the surface of the nanoparticles. Finally, the reactivity of the products obtained was evaluated by reactive iron content analysis Fe (0) and the nitrate reduction capacity in the aqueous phase, in order to corroborate the conservation of the reactive nucleus in response to the functionalization of the materials and the different reducing capacities attributed to the various synthesis methodologies used.

CHAPTER 2

Preparation of air stable nanoscale zero valent iron functionalized by ethylene glycol without inert condition

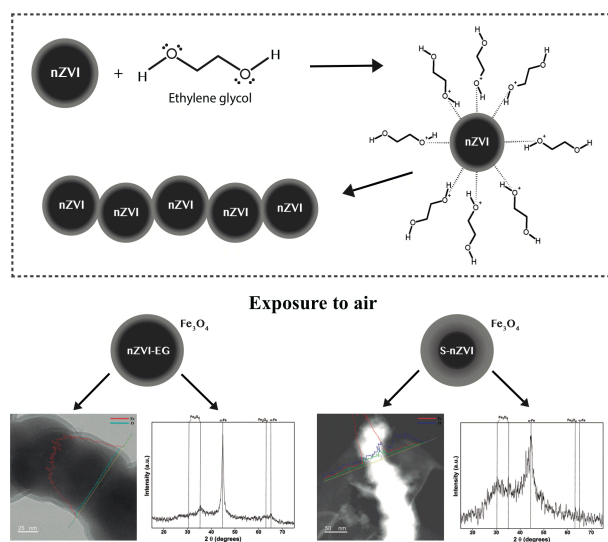
Claudio Adrian Ruiz-Torres^a; René Fernando Araujo-Martínez^a; Gabriel Alejandro Martínez-Castañón^a; J. Elpidio Morales-Sánchez^a; Jesús María Guajardo-Pacheco^a; Jesús González-Hernández^b; Tae-Jin Lee^c; Hyun-Sang Shin^c; Yuhoon Hwang^c; Facundo Ruiz^a

^aFacultad de Ciencias, Universidad Autónoma de San Luis Potosí (UASLP), Avenida Manuel Nava 6, Zona Universitaria, CP. 78290 San Luis Potosí, SLP., MÉXICO

^bCentro de Ingeniería y Desarrollo Industrial (CIDESI), Av. Playa Pie de la Cuesta No. 702. Desarrollo San Pablo. C.P. 76125 Santiago de Querétaro, Qro. MÉXICO.

^cDepartment of Environmental Engineering, Seoul National University of Science and Technology, 232 Gongreung-ro, Nowon-gu, Seoul 01811, Republic of Korea

Graphical abstract



2. ABSTRACT

The use of nanoscale zero-valent iron has been widely studied in recent years for potential application in environmental engineering, due to its affinity for a large number of contaminants, which may be in aqueous or solid phase, and for its abundance, which makes it an attractive tool for environmental remediation. However, there exist some variables in the production of nZVI that complicates the generation of the material, such as the complex methodologies of synthesis and the cost of inert conditions, which have the purpose of preventing the oxidation of the material and reducing the instability of the material under ambient conditions. As a simple and economical synthesis methodology, this work presents an optimized method to synthesize functionalized nanoscale zero-valent iron (nZVI) using ethylene glycol

without need for inert conditions. The coordination of iron ions during the nZVI-EG synthesis and the functionalization mechanism of the nanoparticles were identified by UV-Vis absorption spectroscopy and Fourier transform infrared spectroscopy (FTIR). Functionalized nZVI showed increased dispersibility due to the effects of steric repulsion between the grafted polymers. Ethylene glycol functionalized nZVI showed stability against oxidation during dry atmospheric condition, while significant oxidation was observed in the case of unfunctionalized nZVI. This result was also correlated with actual capacity for contaminant reduction. Therefore, the possibility was verified of using ethylene glycol in an effective surface modification method to prepare air stable nZVI for environmental remediation.

KEYWORDS: Ethylene glycol; nanoscale zero-valent iron (nZVI); functionalization; colloidal stability

2.1 INTRODUCTION

Environmental nanotechnology provides novel tools for remediation based on the synthesis and application of advanced materials that can be functionalized; the process of functionalization optimizes material environmental application, allowing material to act as a contaminant immobilizer in the environment or promoting contaminant degradation [2,3]. A good example is the use of zero-valent iron nanoparticles (nZVI). Because of their high surface area and standard redox potential ($E^0 = -0.44$ V), these materials allow a high rate of reactivity with contaminants via electron transfer during the oxidation of Fe^0 to Fe^{2+} and eventually Fe^{3+} ; this makes these materials efficient reducing and oxidizing agents [9,10] and provides specific affinity for toxic contaminants in aqueous systems [11]. Examples include chlorinated organic solvents, organochlorine pesticides, organic dyes [12–14], and metal ions such as Pb (II), Cu (II), Ni (II) and Cr (VI) [15–19].

Nevertheless, in the application of nZVI to environmental nanotechnology, the stability plays an important role due to high material tendency to react in response to large surface area; such materials are usually unstable when exposed to the air. Moreover, in the synthesis and handling of nZVI, this material is widely known to form an iron oxide thin layer around the particle called core-shell; this layer is established by interaction of the metal core with oxygen present in the surrounding environment, creating a passivation of the surface that can take different crystalline structures such as Wüstite (FeO), magnetite (Fe_3O_4), maghemite ($\gamma-Fe_2O_3$) or Goethite ($\alpha-FeOOH$) [4–7]. The main function of this layer is to avoid the additional oxidation of the particle [8].

However most authors report that, in order to avoid oxidation as much as possible, the synthesis and application of nZVI must make use of inert conditions during the manipulation of the material. On the other hand, the implication of

inert conditions in the synthesis process is a highly cost method, which hinders the development and application of this material in real cases. In relation to this highly relevant fact of nZVI production, it is extremely important to find new ways to stabilize and protect nZVI in the presence of air, where they are highly sensitive to oxygen. For this reason, nanomaterial surface modification is a widely studied area and has great interest because it can provide tools to modify the interactions that materials may have with the surrounding environment [38]. Changes of stability, compatibility, and reactivity are some examples of modifications in materials via a coated surface; such modifications in response incur an increase in potential applications.

Coating techniques can generally be divided into two large groups: first, coating of nanomaterials by use of inorganic materials such as precious metals (Ag, Au, Pt, Pd) [39–42] and silica [43]; second, the coating of nanomaterials by use of organic shields such as surfactants or polymers [44,45]. Researchers have emphasized the latter group in recent years, and advances in polymer nanotechnology have found new and different methodologies to stabilize nanomaterials as protective agents [46,47]; these agents have been applied in the development of systems of organic-inorganic composites. By optimizing material properties using nanoparticle functionalization, it is possible to drastically increase the applicability of iron nanomaterials. Besides this, it has been found to be possible to provide a stable material for the protection of a polymer layer, preventing its reaction with oxygen present in the environment, while preventing agglomeration in solution [48,49].

The modification of the surface of nanomaterials by use of organic compounds has been achieved by different types of synthesis methodology; however, in general the functionalization occurs through an electrostatic interaction among the molecules of the polymer used during the synthesis and the materials because there exists a certain affinity of the functional groups contained in the binding molecules with inorganic surfaces; as a result, there is an attraction among the terminal groups contained in the polymer brushes, which have negative charge, and the surface of the nanoparticles, which have positive charge induced by the charges contained in the colloidal system that surrounds the particles in a hydrodynamic radius. Polymers grafted on particles form a protective layer that imparts different properties to the material; increasing the applicability of these materials; as well, it has been reported that the presence of layers of different varieties of polymers, like coated agents, makes it possible to control the size and agglomeration of nanoparticles by varying the concentration, the geometry, and the terminal groups of the polymers [31]; this is due to the effects of electrostatic repulsion or steric repulsion between the polymers grafted from each particle. On the other hand, the main interest in the functionalization of nZVI in this work is the fact that the protection of the nanoparticles is closely related, so the functionalization of these nanoparticles can prevent the excessive oxidation of the nanomaterial under ambient conditions by the presence of a polymeric protective layer that prevents the reaction with oxygen present

in the environment, avoiding a high rate of nZVI corrosion in the particles, which corrosion would greatly reduce material reactivity and applicability.

In this work, ethylene glycol (EG) was used as a coating agent to provide air stability to synthesized zero-valent iron nanoparticles and to control their corrosion during synthesis and drying. The functionalization led to better applicability of the material due to the modification of its surface, increasing nanoparticle dispersibility in aqueous media. To corroborate the advantages involved in the functionalization of the material, nZVI were obtained in the presence and absence of the coating agent; simple (S-nZVI) and stabilized (nZVI-EG) nanoparticles were obtained. The synthesis of the nanomaterials was carried out by a method of chemical reduction of aqueous ferric salts, which were functionalized with ethylene glycol at room temperature without inert conditions. In order to identify the nZVI functionalization mechanism, the functionalized nZVI sample was analyzed by ultraviolet–visible (UV–Vis) absorption spectroscopy, Fourier transform infrared spectroscopy (FTIR). In addition, the dispersibility of the nanomaterials with and without functionalization was tested by sedimentation test.

Moreover, the samples nZVI-EG and S-nZVI were dried under anaerobic conditions (nZVI-EG₁ and S-nZVI₁) and aerobic conditions (nZVI-EG₂ and S-nZVI₂), in an attempt to compare and identify the degree of oxidation present in nanoparticles in the presence and absence of a functionalizing agent in two different mediums, where the fundamental role of the coating agent is to inhibit contact of the material with oxygen present in the air and the eventual consumption of the metal core of iron in the particle, generating a greater environmental stability and manipulation of the material. The degree of oxidation was evaluated using X-ray diffraction (XRD), High-resolution transmission electron microscopy (HR-TEM), and energy dispersive spectrometry (EDS). The reactive iron content was quantified by measuring the hydrogen (H₂) gas produced by acid digestion. The reactivity of zero-valent iron nanomaterials, which is directly proportional to the Fe(0) content, was analyzed by nitrate reduction.

2.2 MATERIALS AND METHODS

2.2.1 Synthesis and functionalization of nZVI

In this work, employing a strong reducing agent such as sodium borohydride, zero-valent iron material synthesis was carried out by aqueous chemical reduction method of a ferric salt. nZVI were synthesized in a beaker at regular atmospheric conditions; this was in contrast to most synthesis methods that have been reported [2,15,34–37], demonstrating a low-cost methodology for nanoscale zero-valent iron production. First, 50 ml of 0.05M FeCl₃ was dissolved in deionized water and stirred at 800 rpm for 5 min. Later, 0.4 ml of EG was added under stirring for another 10 min. Finally, 0.05 M of NaBH₄ was added to the vessel. The obtained product is a black precipitate, which

corresponds to zero-valent iron nanoparticles. Subsequently, the product was washed three times with ethanol to remove the unreacted ions present in solution. S-nZVI was synthesized under similar conditions without EG addition during the synthesis. The nZVI-EG₁ and S-nZVI₁ samples were dried in anaerobic conditions in an anaerobic chamber for 24 h (N₂:H₂ 95:5). Moreover, in order to compare the air stability and iron core consumption of the two different samples with and without functionalization to atmospheric and inert dried conditions, and their oxidation rate and reactivity to nitrate reduction, samples nZVI-EG₂ and S-nZVI₂ were dried under aerobic conditions in an open container for 24 h.

2.2.2 Physical characterization methods

The coordination of iron ions during nZVI-EG synthesis and the functionalization mechanism of the nanoparticles were identified by UV-Vis absorption spectroscopy and Fourier transform infrared spectroscopy (FTIR) characterization techniques. UV-Vis absorption spectroscopy was performed using an S2000-UV-Vis spectrometer from OceanOptics Inc.; Fourier transform infrared spectroscopy (FTIR) was performed using a Shimadzu IRAffinity-1.

Morphological analysis was conducted using a transmission electron microscope (TEM). TEM images at 100 kV were obtained using a JEOL-1230; HR-TEM microphotographs were captured on a JEM-2200FS field emission transmission electron microscope at an acceleration voltage of 200 kV. An Energy Dispersive Spectrometer scanning line (EDS) was used to detect the element distributions of Fe and O; this was performed by TEM equipment (JEM-2200FS).

Structural changes of nZVI during dry step were characterized by X-ray diffraction patterns. XRD were recorded with a GBC-Difftech MMA diffractometer with filtered CuK α ($\lambda = 1.54$ Å) radiation. To corroborate the presence of iron zero-valent (α -Fe) and iron oxide (Fe_xO_y), and to perform phase quantification and crystallite size estimation, X-ray data refinement was obtained by subjecting the XRD data to Rietveld refinement [50] using the program MAUD .

Dispersibility of nZVI particles was determined by sedimentation analysis using a UV-Vis spectrophotometer (Cary 50, Agilent Technologies Inc., USA). The dispersions were shaken but not sonicated prior to the experiment. Then, the samples were transferred into a 1-cm plastic cuvette and capped to prevent further oxidation during the sedimentation test. The absorbance of the diluted samples was monitored as a function of time, with the optical absorbance at 508 nm, to obtain the sedimentation curve. The sedimentation curves were interpreted using the following equation [32].

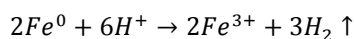
$$I_t = I_0 e^{-t/\tau}$$

where I_t is the absorbance of solution at time t , I_0 is the initial absorbance, and τ is the characteristic time.

2.2.3 Reactivity measurements

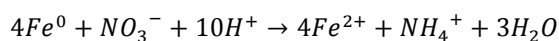
2.2.3.1 Reactive iron contents

Following the methodology reported by [26], the reactive iron content among prepared nZVI samples was determined by quantification of hydrogen gas (H₂), which is produced during the acid digestion of the sample according to the following reaction, where only the Fe (0) present in the sample will produce H₂. A solution of concentrated hydrochloric acid (37%) with a concentration of 1.5 g/l of nZVI is put in a 22 ml vial. The vial is purged and capped to allow the reaction to proceed for 24 hrs. The quantification of H₂ was performed by using a gas-tight syringe removing 0.5 ml of the headspace in the closed vial; the sample was analyzed by gas chromatography. Later, the total iron concentration in solution was measured by atomic absorption spectrometry (AAAnalyst 200, PerkinElmer, USA) and then compared with the H₂ value obtained from the calculation of the Fe (0) content of the sample.



2.2.3.2 Nitrate reduction capacity

The reducing reactivity of the nZVI samples was determined by the reduction of nitrates to ammonia. The experiments were carried out in a 50 ml bottle. 25 mg of nZVI was added to the bottle, along with 23 ml of deionized water; the pH of the solution was adjusted to 5 by adding 1 ml of 250 mM acetic acid buffer solution; the vial was purged with nitrogen and sealed. Then, 1 ml of the nitrate stock solution (625 mg NO₃-N/L) was injected. The final concentrations in the solution are 12.5 mg NO₃-N/L and 1000 mg Fe/L. The bottle was stirred for 1 min for the dispersion of the material and placed in shaker at 150 ppm. Samples were taken periodically and filtered through a 0.45 μm membrane; the ammonia content was immediately analyzed. Ammonia analysis was conducted based on the procedure described in previous research [51].



2.3. RESULTS AND DISCUSSION

2.3.1 nZVI functionalization by ethylene glycol

2.3.1.1 Functionalization mechanism

In order to identify the mechanisms involved in the functionalization, the sample was characterized by ultraviolet–visible (UV–Vis) absorption spectroscopy and FTIR spectroscopy. In Figure 1A, the absorption spectrum of the FeCl₃ solution shows a band at 300 nm, which corresponds to the presence of Fe³⁺ ions. Subsequently, when the stabilizing

agent is added to the solution, a modification of the absorption band is observed, which can be directly attributed to the interaction of Fe^{3+} with EG, forming a relative stable complex $[\text{Fe}(\text{EG})]^{3+}$. The addition of the reducing agent NaBH_4 initiates the nucleation process of nZVI. In the absorption spectrum belonging to nZVI-EG, there is a modification in the absorption band, which is completely different from the initial solutions having a maximum absorption at 250 nm.

Figure 1B shows the FTIR analysis, which was performed with the purpose of comparing the infrared spectra of neat EG and EG stabilized nZVI; this was done to characterize the changes in the chemical bonds that occur due to the functionalization of nZVI. The EG spectrum presents a band at 3307.3 cm^{-1} (O-H groups stretch band), a band at 2860 cm^{-1} (asymmetric C-H stretch deformation), a band at 2930 cm^{-1} (symmetrical C-H stretch deformation), a band at 1648.5 cm^{-1} (OH groups flexural vibration of the water molecules absorbed in the sample), a band at 1400.9 cm^{-1} (flexural strain of C-H group), and a band at 1157.5 cm^{-1} (extension of O-H and C-O-H).

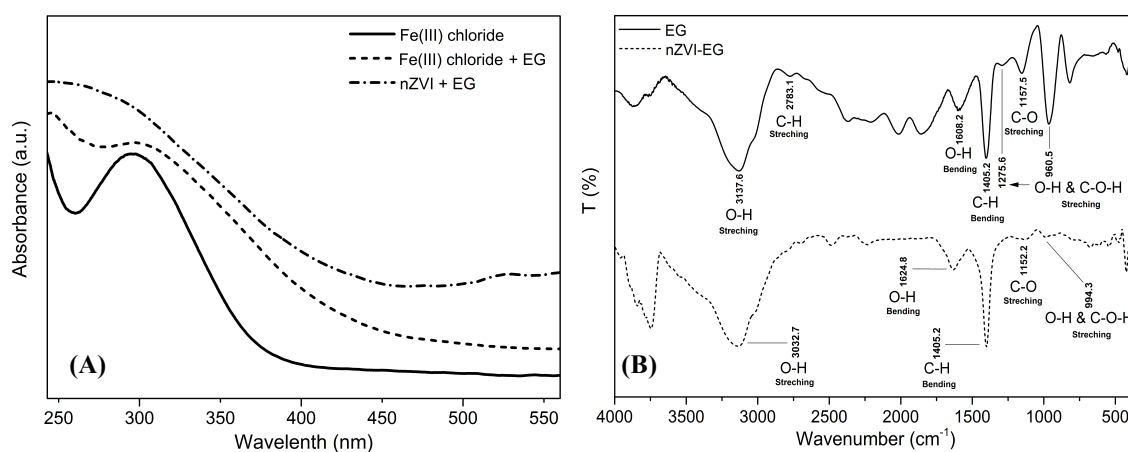
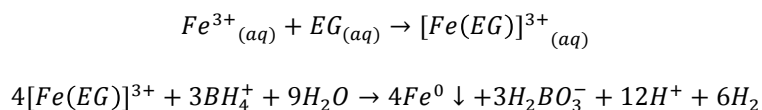


Figure 1. A) UV–Vis aqueous absorption spectra of FeCl_3 , $[\text{Fe}(\text{EG})]^{3+}$ and spectra of nZVI functionalized with EG. **B)** FTIR spectrum of EG and nZVI-EG.

In the FTIR spectrum of nZVI-EG, the characteristic bands of EG found at 3307.3 , 2992.7 , and 1400.9 cm^{-1} are displaced to 3147.6 , 3025.2 , and 1394.6 cm^{-1} . However, for the case of the deformation by stretching of groups O-H and C-O-H to 994.3 cm^{-1} , there is a noticeable decrease in the intensity of the band. This decrease in the intensity of the vibrational frequency can be associated with the attenuation of the functional COH group due to interaction between the partially positively charged surface of the particle and the electron cloud of the last orbitals of the oxygen atom present in the carboxyl group, forming a coordinate covalent bond $\text{O}-\text{Fe}^0$ (schematic Figure) [52].

Based on the results obtained by UV-Vis and FTIR analysis, the functionalization mechanism can be concluded to be as below. First, the iron ions coordinated through the addition of EG molecules; after that, NaBH_4 was added to the

solution and Fe (III) ions were reduced to Fe⁰, starting the nucleation process and particle formation according to the following possible reaction.



Interaction is carried out by the intermolecular Van der Waals forces between the positive partial charge of the surface of nZVI (due to the presence of positively charged groups that surround the zero-valent iron nanoparticles) and the negatively charged COH groups present in EG, leaving grafted polymers on the particle surface and thereby generating a surrounding layer that modifies the interactions of the material with the medium and gives stability against the presence of oxygen under atmospheric conditions (Figure 2) [53]. Furthermore, because of the high solubility of the polymer in different solvents such as water, and organic polar and nonpolar solvents, an increase in the dispersibility of the material can be predicted because of the EG coating process. In response, there is a generation of an inert hydrophilic surface with less adhesion due to the terminal OH groups, which do not adhere to the surface of the functionalized target, modifying the interaction of this material with the medium [38,54].

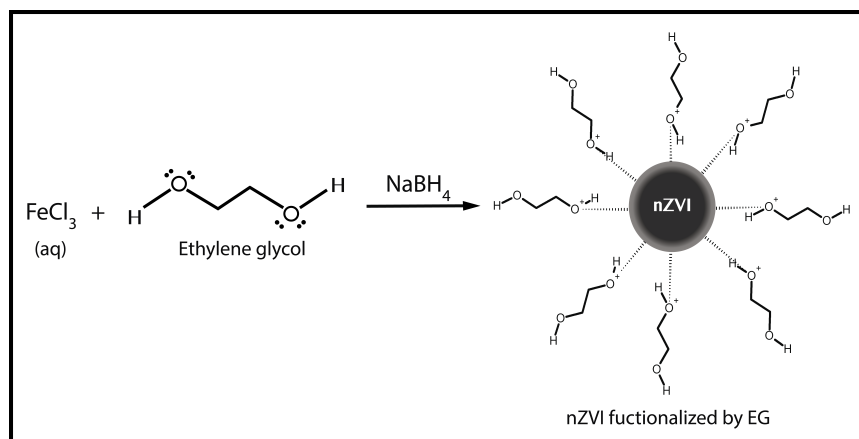


Figure 2 Schematic illustration showing Fe³⁺ coordination process and functionalization of nZVI by EG.

2.3.1.2 Structural characterization

TEM images of the materials with and without functionalization display particles with quasi-spherical morphology, with well-aligned aggregates forming zero-valent iron nanochains. The individual particles of nZVI-EG and S-nZVI show average diameters of 54.88 and 76.72 nm with coefficients of variation (CV) of 27.84 and 31.43%, in the size range of 16.96-100.20 nm and 24.50-165.35 nm respectively (Figure 3 A-B). The smaller average diameter and narrower size distribution could be obtained by surface modification with EG. This is due to the coordination of Fe³⁺ ions during the synthesis as well as the functionalization of the particles surface by the grafted polymers brushes. The arrangement of zero valent iron nanoparticles in chain structures is mainly caused by the magnetic dipole-dipole

interactions of the particles, which generate spherical nanoparticle addition, and an arrangement of the particles in a magnetic cluster with chain morphology [55] (Figure 3 A-B). Figure 3C provides a conceptual model of the nZVI interactions that form the ZVI nanochains.

The use of EG during the synthesis has no great effect on the size control during the synthesis due to the fact that in the process of nucleation of the material, the primary particles, with sizes that are very small with respect to the final sizes, usually have interaction energies or barriers of very low energy and higher kinetic energy values; on the other hand, the natural magnetic properties of these particles promotes attraction between them, and the absence of high repulsion values leads to a greater facility to agglomerate and grow to a certain size, where they present greater stability. As the diameter of the particles increases the energy barrier also increases; the kinetic energy is decreased and, in addition, due to the presence of electric charges on the particle surface, that make up the nZVI hydrodynamic radius, is possible avert complete contact and avoiding the agglomeration and growth of the particles to mean sizes of >54.88-76.72 nm; this size control adds to the magnetic effect, generating an attractive-repulsive force and an arrangement of the particles in a magnetic cluster.

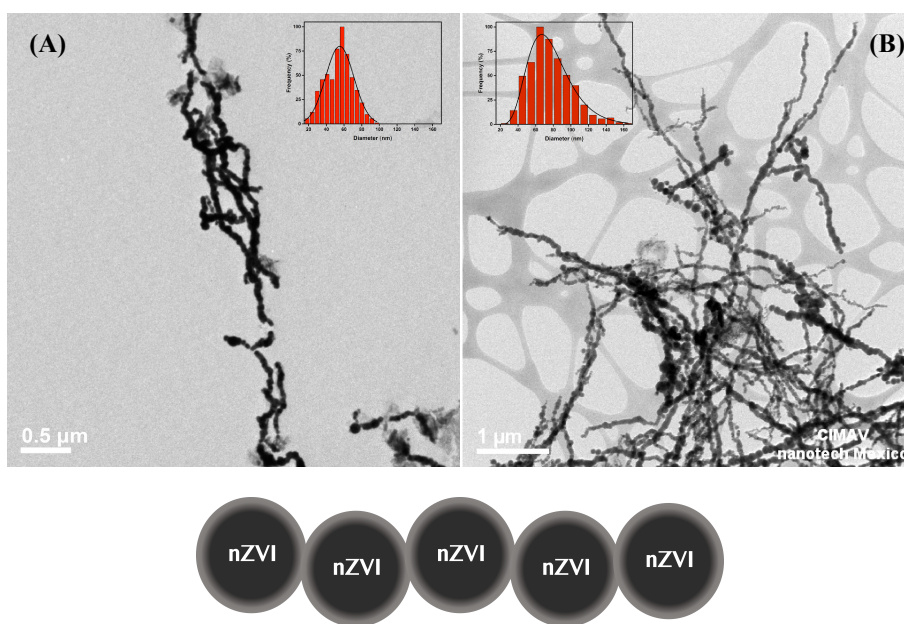


Figure 3. A-B) TEM photomicrography of nZVI-EG and S-nZVI and their corresponding histograms. **C)** Schematic model of ZVI nanochains.

2.3.2 Increased dispersibility by nZVI functionalization

The stability of the materials was analyzed by sedimentation analysis in order to compare the increase in dispersibility of the nanoparticles in solution due to the modification of their surface by the presence of grafted polymers. The curve was further analyzed using the one-phase decay equation, as described in our previous study.

$$I_t = I_0 e^{-t/\tau}$$

In Figure 4 it is possible to observe a high sedimentation rate for S-nZVI associated with the rapid aggregation of the particles. S-nZVI has an absorbance of 0.045 at its plateau, which means that more than 95% of nZVI will settle down during the sedimentation experiment. On the other hand, 73% of nZVI would settle down in the case of surface functionalized nZVI-EG. Moreover, the characteristic times τ for S-nZVI and nZVI-EG are calculated at 14.7 and 35.8 min, respectively, which means that nZVI-EG is much more stable than S-nZVI.

The slow sedimentation rate can be explained by the increase in the stability of the material in response to the functionalization of the particles and the reduction in the rate of aggregation of these particles due to effects of steric repulsion between the grafted polymers. The increase in dispersibility is due to the fact that the polymeric brush, which is only attached at one end to the surface of the particle, has another OH terminal group that is not bound to the surface of another particle and is free to interact with the surrounding medium. This OH group is highly soluble in polar solutions, promoting the dispersibility of the particles, which are covered with a polymer layer of this composition; this layer may be assumed to also increase the interactivity with contaminants to be removed or reduced.

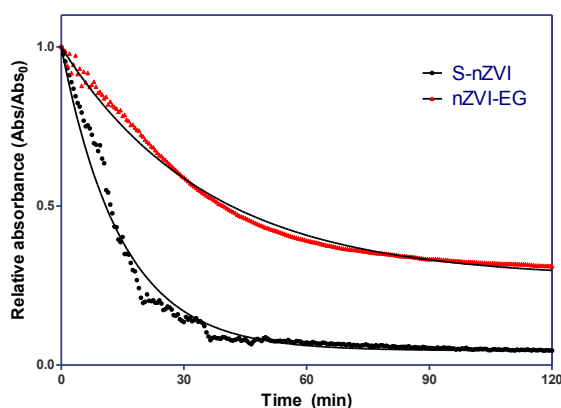


Figure 4 Sedimentation curves of nZVI and nZVI-EG

2.3.3 Air stability of functionalized nZVI

The samples nZVI-EG₁ and S-nZVI₁ dried under anaerobic conditions and the samples nZVI-EG₂ and S-nZVI₂ dried under aerobic conditions were analyzed by XRD, HR-TEM, EDS, reactive iron content analysis, and nitrate reduction in order to demonstrate the consumption of the reactive metallic iron core and the oxygen increase present in the core-shell composed of iron oxide due to oxidation of the material in response to the absence of an EG protective layer and the loss of the reducing capacity of the nanoparticles.

2.3.3.1 Structural characterization - XRD

Using the Rietveld method, the XRD information was refined: the amount of zero-valent iron and the core-shell were quantified in the samples. The X-Ray spectrum of nZVI-EG₁ and its Rietveld refinement show characteristic peaks of cubic phase α -Fe located at 44.8° and 65.8°; these are indexed as the (110) and (200) planes (JCPDS Card No. 79-0417). For the case of sample S-nZVI₁, it is possible to see the existence of zero-valent iron (α -Fe) and the presence of iron oxide (Fe_xO_y) crystalline phases in the XRD, which similarly shows peaks belonging to the crystallographic phase α -Fe indexed in the planes. However, the peaks at 35.9 and 62.9° correspond to the crystallographic cubic phase magnetite (Fe_3O_4), indexed in the planes (311) and (411) (JCPDS 06-0696), coinciding with the presence of magnetite and evidencing the layered structure of nZVI, which consists of a body-centered cubic (bcc) α -Fe metal core encapsulated by a thin oxide shell [28,29] (Figure 5).

For the samples dried in aerobic conditions, the XRD result corresponding to nZVI-EG₂ shows an α -Fe peak with an intensity similar to that of samples described above. The spectrum for S-nZVI₂ shows a remarkable difference with respect to the other samples: it shows a decrease in the intensity at the peak corresponding to α -Fe and an increase in the intensity of the diffracted peaks; this is associated with the presence of magnetite located at 30.3 and 35.8° in planes (200) and (311) (JCPDS 06-0696). The presence of magnetite is due to the corrosion of the reactive iron core and the transformation to the Fe_3O_4 phase (Figure 5). In the same way as in the quantification of the crystalline phases, we see an interesting decrease in α -Fe and an increase in magnetite (Table 1).

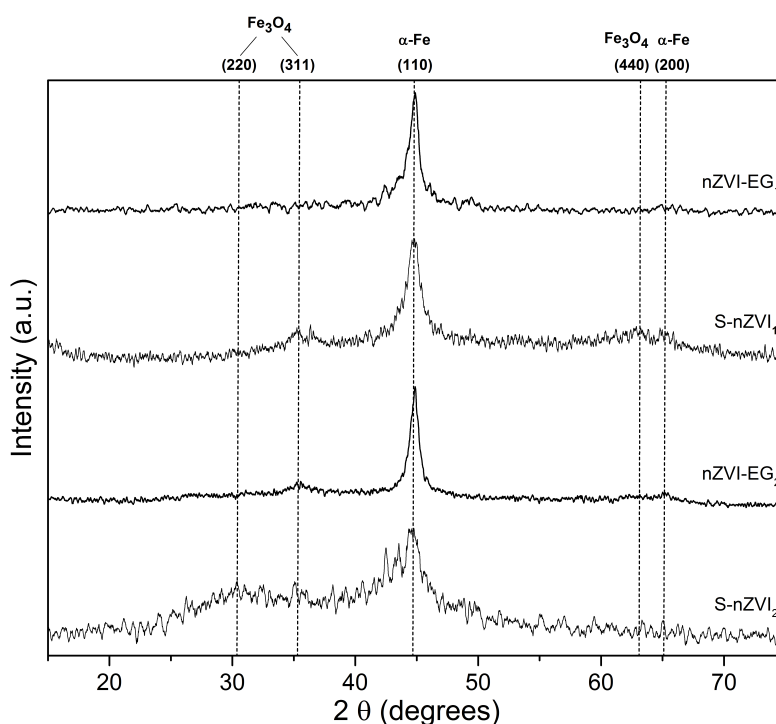


Figure 5 Powder X-ray diffraction (XRD) patterns of nZVI and functionalized nZVI dried in anaerobic and aerobic conditions.

The transformation and evolution of nZVI to iron oxides, especially magnetite is a common phenomenon in atmospheric conditions, where it has been widely reported that there is a decrease of the peaks corresponding to α -Fe until their eventual disappearance and that there is an increment of the magnetite phase according to the degree of oxidation of the sample [8].

Table 1

Rietveld refinement of a sample zero-valent iron nanochain with and without EG.

Sample	α -Fe % in weight	Fe ₃ O ₄ % in weight
nZVI-EG ₁	98.87	1.13
S-nZVI ₁	78.28	21.72
nZVI-EG ₂	85.17	14.83
S-nZVI ₂	44.98	55.02

However, there is a difference between samples dried under anaerobic and aerobic conditions because, during the synthesis of nZVI without surface modification in oxic water, O₂ groups were absorbed on the surface of the particles; these groups are possibly preserved even after a process such as washing; likewise, more O₂ groups present in the air are absorbed during drying. Those groups are able to react with the reactive iron in the material, oxidizing it and consuming its reactivity, while forming a higher amount of magnetite.

In contrast, for the functionalized samples, the protective layer inhibits almost entirely the addition and interaction of these groups on the surface of the particles, preserving the majority of the metal core. The remarkable difference in the oxidation rate between the S-nZVI₁ and S-nZVI₂ samples is explained as being due to the O₂ groups that were absorbed on the surface of the material reacting with the hydrogen contained in the atmosphere of the anaerobic chamber and forming water; this water is subsequently removed from the chamber, preventing any reaction with the zero-valent iron contained in the particles.

2. 3.3.2 Morphological characterization – TEM and EDS

Similarly, TEM images of the samples dried under aerobic conditions were obtained to evaluate sample morphology. The sample nZVI-EG₂ presents a behavior similar to that described in the previous section, in which the sample was dried in anaerobic conditions, indicating that this sample is not significantly affected by corrosion effects due to the efficiency of the functionalization (Figure 6A).

In the case of S-nZVI₂, a conservation of the nanochains is observed, which may explain the occurrence of the consumption of the metallic nucleus and the increase of iron oxides while maintaining the same morphology of

particles. Moreover, in the upper part of the image, some structures in the form of needles are shown; these are characteristic of a more advanced iron oxidation process (Figure 6B). Nevertheless, in the XRD information, no peaks other than that of magnetite are shown, which may be interpreted as representing an amount of a type of iron oxide other than Fe_3O_4 , one that is insufficient to be detected by X-ray diffraction.

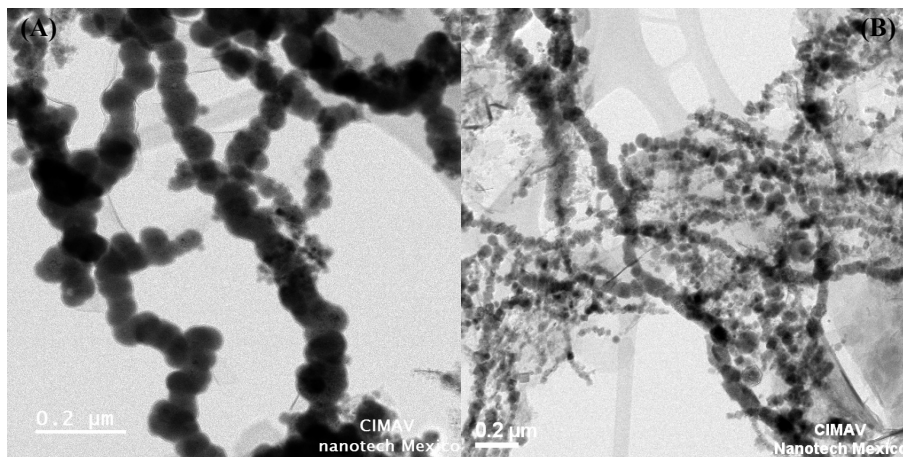


Figure 6 A-B) TEM photomicrography of nZVI-EG₂ and S-nZVI₂.

Figure 7 present HR-TEM images of the different samples, showing changes due to drying in anaerobic and aerobic conditions. The nanoparticles are composed of a dense core surrounded by a thin shell; the magnetite exhibits markedly less contrast than does the zero-valent iron dense core. The cases of nZVI-EG₁ and nZVI-EG₂ showed similar behavior in the core-shell, with average thickness values of 4.48 and 4.94 nm, respectively, indicating a non-significant increase in thickness due to oxidation of the reactive iron upon exposure to atmospheric conditions (Figure 7;A-B).

On the other hand, the thickness of the core-shell of S-nZVI₂ significantly increased compared to that of S-nZVI₁. S-nZVI₁ shows a thickness of core-shell of 5.76 nm (Figure 7C). The S-nZVI₂ sample showed a higher corrosion of particles and a higher consumption of the iron core, leading to an eventual increase in the core-shell thickness. Figure 7D shows the remarkable increase in the thickness of the iron oxide layer, in contrast to those of the other samples, presenting a value of 11.89 nm. This result demonstrates the instability of the nZVI, in the absence of functionalization, against environmental conditions [8,56].

Energy Dispersive Spectroscopy scanning line (EDS), used to analyze iron nanoparticle structure composition along nanoscale ZVI chain in the samples subjected to drying under aerobic and anaerobic conditions; this was an attempt to demonstrate the predominance of the α -Fe core, which is surrounded by a thin iron oxide core-shell for nZVI-EG dried even in aerobic conditions; EDS results also show the consumption of the metallic nucleus due to oxidation and the increase of the oxygen present in the core-shell in response to the absence of a protective layer for non-functionalized nZVI.

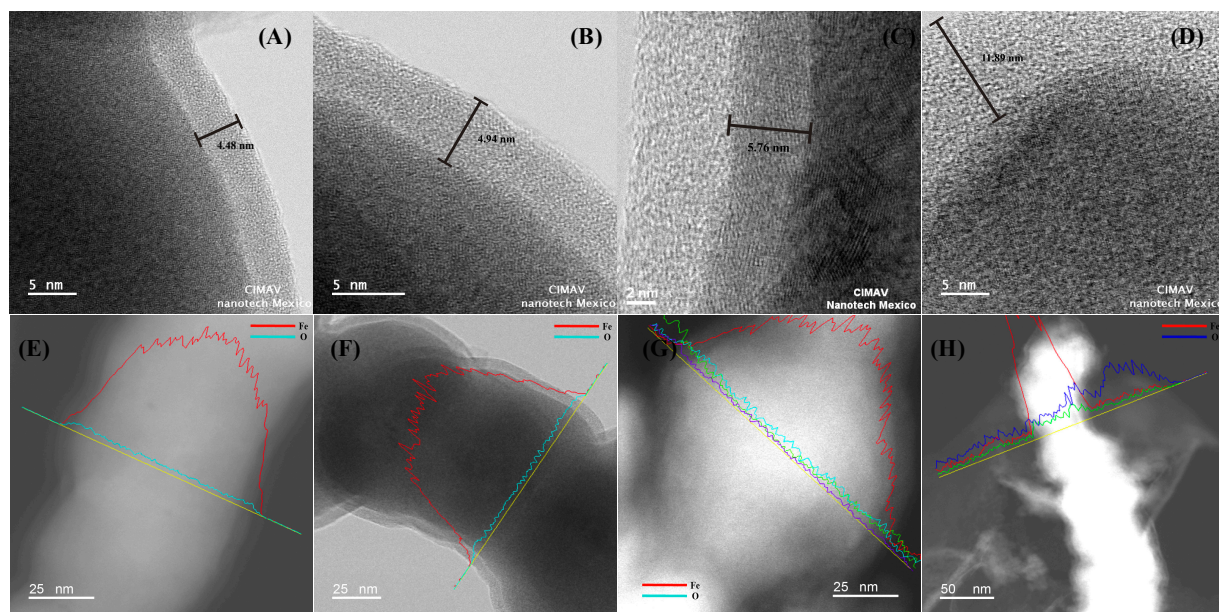


Figure 7 A-D) HR-TEM photomicrography of nZVI samples (A: nZVI-EG₁, B: nZVI-EG₂, C: S-nZVI₁, D: S-nZVI₂). **E-H)** Energy dispersive spectrometer scanning line (EDS) of nanoparticles with and without functionalization dried in aerobic and anaerobic conditions (E: nZVI-EG₁, F: nZVI-EG₂, G: S-nZVI₁, H: S-nZVI₂).

The spectrum of the dispersed energy scanning line is obtained at three selected points in the area of interest on the sample, forming a Y-modulated signal; this is a rough indication of the number of, and the amounts of, elements present with respect to the spatial location along the line. We plotted a concentration profile to analyze the Fe and O diffusion in the nZVI core and determined the interface between these.

EDS analysis for nZVI-EG dried under anaerobic conditions shows at the center of the particles the Fe spectrum, with a high intensity and a predominance (95.97%) in the sample that correspond to an iron metal core of the particles; moreover, it is possible to observe quite less of a proportion and spectrum intensity of corresponding oxygen (4.03%). Nevertheless, the iron content and spectrum intensity drop as the edges of the particle (81.12 and 63.89%) are approached; this is in contrast to the increment of the amount of oxygen at the edges (18.88 and 36.11%) due to the presence of the iron oxide core-shell surrounding the α -Fe core and forming an nZVI structure (Figure 7;E). The EDS spectra corresponding to samples S-nZVI₁ (Figure 7;G) and nZVI-EG₂ (Figure 7;F) show modulation of the Fe and O signal, very similar to the first spectrum described. Thus, like the information provided by XRD, TEM, and HR-TEM, the behavior and degree of oxidation between these materials show no noticeable changes.

For the last case of S-nZVI₂, the most notable differences are the change in the uniformity of the signal corresponding to Fe and the increase in the intensity of the spectrum of O. Having values of Fe in the center (68.80%), showing an interesting decrease in the proportion of the metal core and a predominance of the content of O with respect to Fe in the

whole particle analyzed, values of (Fe-O; 27.26-72.74% and 30.69-69.3%) were reached at the edges of the structure (Figure 7;H). Table 2 shows the element distribution of Fe and O in the samples.

Table 2
Composition of EDS points in Figure 7 E-H, wt%.

Elemento	Fe (%)			O (%)		
	1	2	3	1	2	3
Spectrum						
nZVI-EG ₁	81.12	95.97	63.89	18.88	4.03	36.11
nZVI-EG ₂	62.4	87.15	79.9	37.6	12.85	20.1
S-nZVI ₁	81.34	83.15	62.06	18.66	16.85	37.94
S-nZVI ₂	27.26	68.8	30.69	72.74	31.2	69.31

2.3.3.3 Effect of oxidation on nZVI reactivity

The amount of reactive iron remaining after drying under anaerobic and aerobic conditions indicates the degree of oxidation of the sample and its stability. Analyses of this parameter for nanoparticles dried in the anaerobic chamber show values of preservation of Fe(0) of 84.6 and 78.9% for the nZVI-EG₁ and S-nZVI₁ samples, respectively, with the loss of a little more than 15% of the reactive nucleus being due to oxidization during the synthesis; the synthesis is carried out in oxic water in the open container and in the absence of inert gas. The small difference of Fe(0) between both materials shows the better stability of the particles due to the functionalization.

For cases corresponding to samples dried under aerobic conditions, there is a marked contrast between the obtained values of reactive iron. The values of nZVI-EG₂ of 80.2% and S-nZVI₂ of 20.7% demonstrate instability against oxidation during drying (Figure 8A). Furthermore, despite the conditions described above, a high percentage of Fe(0) was obtained in the functionalized samples (nZVI-EG₂), with a loss of 4.4% of reactive iron between both demonstrating the efficiency and protection of the composite layer by the polymers in the aerobic environment. In fact, the calculated percentages of Fe(0) strongly agree with the quantification of the crystalline phase α -Fe in the XRD analysis, corroborating the zero-valent iron identity.

Similar results were obtained in the nitrate reduction test. Ammonia, the main reaction product, was monitored through the reaction period, as shown in Figure 8B.



The nZVI sample, prepared in anaerobic conditions, showed more than 78% of nitrate reduction in an hour for both cases, while only less than 7.1% of nitrate could be reduced to ammonia in S-nZVI₂, which is dried in aerobic conditions without functionalization. On the other hand, an almost similar performance, 74% of nitrate reduction in 1 h,

was obtained when using nZVI-EG₂, which is dried in aerobic condition with functionalization. Dissolved iron content during nitrate reduction are presented in Figure 8C. S-nZVI₂ produce the lowest amount of soluble iron indicating lower reactive iron content and nitrate reduction capacity. This result is in very close agreement with the reactive iron content analysis, and clearly indicates the effectiveness of nZVI functionalization by EG at preventing oxidation during the preparation of nZVI without inert conditions. Furthermore, the reaction kinetics was not hindered by the addition of the organic functionalization agent, EG, which also verifies the possibility of using EG in effective surface modification method for nZVI.

In this study, the effectiveness of ethylene glycol in a surface modification method for the synthesis of air-stable nZVI without inert conditions was investigated. Ethylene glycol helped coordinate with iron ions, which were further reduced to Fe⁰; then, the functionalization provided stability against the presence of oxygen, as well as high dispersibility in water. It was possible to obtain smaller and narrower size distribution by surface functionalization; this process provided better colloidal stability, which was confirmed by a slower sedimentation curve.

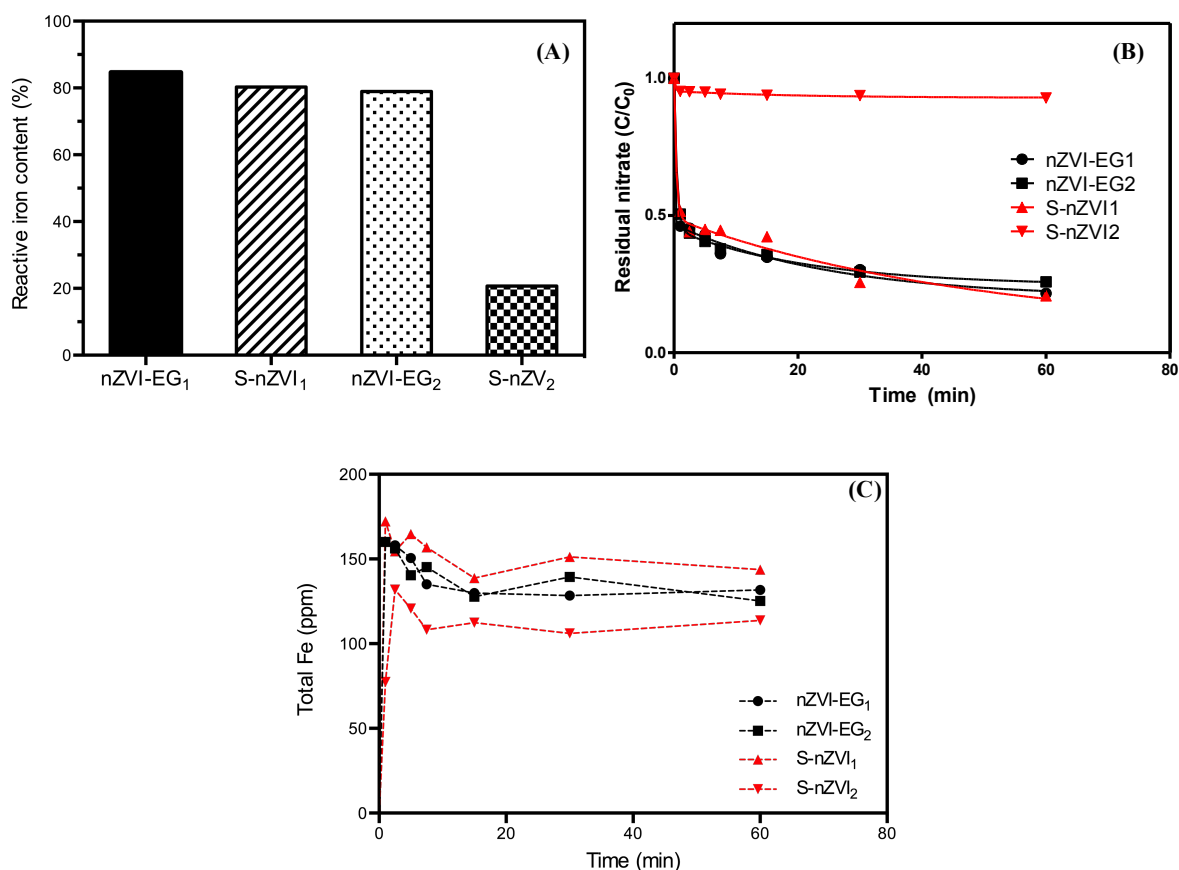


Figure 8. **A)** Reactive iron content of nZVI samples. **B)** Nitrate reduction by nZVI samples. **C)** Dissolved iron concentration during nitrate reduction. (Conditions: 12.5 mg NO₃-N/L and 1000 mg Fe/L, pH 5, T=24±1°C).

2.4 CONCLUSIONS

The ethylene glycol functionalized nZVI also exhibited a protection effect against oxidation in atmospheric conditions. Even though the nZVI preparation was performed without inert condition, the sample was not significantly affected by corrosion due to the efficiency of the functionalization in terms of its morphology as monitored by TEM/EDS and its structure as monitored by XRD. The protection effect of ethylene glycol was also revealed in its contaminant reduction capacity. It was possible to obtain a high percentage of reactive iron and effective nitrate reduction, which indicates the effectiveness of nZVI functionalization by EG at preventing oxidation during the preparation of nZVI without inert conditions. Moreover, the reaction kinetics was not hindered by the addition of the organic functionalization agent EG, which also verifies the possibility of using EG in an effective surface modification method for nZVI.

CHAPTER 3

Ultrasmall and high stable, size controlled nano zero valent iron preparation using non-aqueous solvent with functionalization agent

Claudio Adrian Ruiz-Torres^a; René Fernando Araujo-Martínez^a; Gabriel Alejandro Martínez-Castañón^a; J. Elpidio Morales-Sánchez^a; Jesús María Guajardo-Pacheco^a; Jesús González-Hernández^b; Tae-Jin Lee^c; Hyun-Sang Shin^c; Yuhoon Hwang^c; Facundo Ruiz^a

^a*Facultad de Ciencias, Universidad Autónoma de San Luis Potosí (UASLP), Avenida Manuel Nava 6, Zona Universitaria, CP. 78290 San Luis Potosí, SLP., MÉXICO*

^b*Centro de Ingeniería y Desarrollo Industrial (CIDESI), Av. Playa Pie de la Cuesta No. 702. Desarrollo San Pablo. C.P. 76125 Santiago de Querétaro, Qro. MÉXICO.*

^c*Department of Environmental Engineering, Seoul National University of Science and Technology, 232 Gongreung-ro, Nowon-gu, Seoul 01811, Republic of Korea*

3. ABSTRACT

Nanoscale zero-valent iron (nZVI) has proved to be an effective tool in the applied environmental nanotechnology, where the decrease in particle diameter (<10 nm) provides a drastic change in the properties and efficiency of nanomaterial in water purification. This study reports a new strategy for ultrasmall, <7.5% size distributed functionalized nZVI-EG (1–9 nm), with good crystallinity and a such high colloidal stability, obtaining without inert conditions, as a simple and economical synthesis methodology, employing two stabilization mechanism base on non-aqueous solvent and ethylene glycol (EG) as a stabilizer. The UV-Vis absorption spectroscopy and Fourier transform infrared spectroscopy (FTIR) information suggest the iron ions coordination by interaction with methanol molecules as first stabilization mechanism, subsequently, Posterior to nZVI formation, occurs the particle surface modification by the addition of the organic functionalization agent EG. Size distribution analysis shows an average diameter of 4.23 nm and the predominance of >90% of particles with sizes <6.10 nm. Stability of functionalized nZVI evaluated by sedimentation test and dynamic light scattering technique, demonstrated such a high colloidal stability with a characteristic time of 1993 min, which is explained because of the ultrasmall size and the increment of the dispersibility, due to the effects of steric repulsion between the grafted polymers. The improved properties of the nanomaterial were directly associated with the high contaminant reduction capacity presented.

KEYWORDS: Ultrasmall; non-aqueous solvent; ethylene glycol; stabilization mechanism; nanoscale zero-valent iron (nZVI); high colloidal stability

3.1 INTRODUCTION

The alarming population growth, as well as industrial activities, have led to elevated concentrations of a wide range of contaminants in wastewater and groundwater [1]. For that reason it is important to find new and more efficient technologies in the purification and treatment of water. Zero-valent iron nanoparticle (nZVI) has proved an effective tool for the treatment of wastewater because of its large surface area and specific affinity for toxic contaminants in aqueous systems [11]. However, the need to find materials with greater efficiency in its application persists, which is related to the dimensions and the uniformity of the diameters in these and the anti-aggregation capacity and colloidal stability of the nanoparticles. On the other hand, they need to be obtained through simple and economical synthesis methodologies to become a cost-effective solution in environmental remediation.

There are several reports based on nanomaterials of zero-valent iron with ultrasmall sizes and narrow size distribution (<3-8 nm) using synthetic techniques based on sonochemical decomposition of iron carbonyl, thermal decomposition of iron pentacarbonyl and sonolysis of iron pentacarbonyl, where the mentioned methodologies make use of a stabilizing agent of variable composition which intensifies the reduction and control of particle size [23–25,21]. Notwithstanding, the synthesis techniques mentioned above can be fully classified as extremely complex and expensive methodologies, which require highly controlled conditions, making it impossible to use nZVI as a decontamination agent in environmental purification.

In light of this, in this work, emphasis is placed on the chemical reduction of a ferric salt (FeCl_3) in aqueous phase, using as reducing agent NaBH_4 [4], which results in a remarkable reduction in costs and complexity. However, corrosion during synthesis should be carefully controlled, which implies the need for inert conditions, complicating the methodology. Moreover, several reports that used this methodology, which shows a broad particle size distribution, producing nanoparticles with diameters in the range of 10-100 nm, which average sizes of 50-70 nm, which prove to be characteristic of said synthesis methodology [4,16,26–30].

In order to overcome several issues mentioned above, the use of stabilizing agents of organic origin for the surface modification of the nanomaterials of this type has been studied extensively in the last years, trying to modify the interactions of the particles with the surrounding environment, altering with this the dispersibility of the material in the solvent, the aggregation rate of the magnetic particles and thus the reactivity of the material [26,45]. In the same way, through the use of organic substances during the synthesis of the nanomaterial, it is possible to generate steric repulsion conditions between the particles to control their size, which occurs during the formation of primary particles in the nucleation process, due to the interaction between these and the chains of the polymer used, the latter being grafted onto

the surface of the nanoparticles and stabilizing them, thus avoiding their agglomeration and growth, achieving smaller particle diameters of nZVI (<40 nm). Nevertheless, even when in existing reports is presented a size reduction by the use of coated agent, on average the obtained particles show a broad size distribution ($\pm 2-60$ nm) [31,32], reason why it is deduced a poor control in this aspect. In addition in our previous study, we present the effectiveness of ethylene glycol (EG) as functionalized agent in the obtaining of air stable nZVI and size distribution control (Claudio et al., 2017, submitted), however even with the presence of EG is preserved larges diameters in the particles, which mean that using this methodology is not enough to control the size of the nanoparticles. Persisting the need to obtain ultrasmall nanoparticles with narrow size distribution, which should be obtained through a cost-effective and simple methodology.

In response to this, the modification of the synthesis methodology in question of the type of solvent used has been studied recently, using non-aqueous solvents, more specifically alcohols, as a substitute, providing various benefits during the synthesis of nanomaterials. There are several reports of non-aqueous solvents use for the synthesis of nanoparticles, which have demonstrated that the physical properties of the solvent are directly related to particle stabilization [33–36]. In fact, it is known that viscosity is lineally associated with molecular diffusion [58], so the low viscosity index of alcohols, specifically the case of methanol favors the propagation of the reducing agent and the precursor within the solvent, increasing the uniformity in the reduction and nucleation process. Additionally, the nanomaterials obtaining by means of chemical reduction in low polar solvents promotes the increase in the concentrations of nuclei and small particle sizes [36]. One of the main benefits in the use of non-aqueous solvents in the synthesis of zero-valent iron nanomaterials is the prevention of excessive oxidation of the material, preserving the metallic core of reactive iron and avoiding the use of inert conditions, reducing the costs in the methodology remarkably. However, even with the use of non-aqueous solvent in its entirety, which generates smaller particle sizes as compared to aqueous synthesis, a broad distribution of sizes has been reported [35]. Supplementary, there are counterproductive effects in the use of alcohols as solvents where an inhibition of H-bonding conduce to lower electrostatic stabilization of the nanomaterial in the solvent, inducing the interaction between the particles generating their agglomeration and growth [35,37], by cause of this fact, the non-aqueous solvent methodologies were reported as good methods in nanoparticle size decrease, but it is not enough to obtain ultrasmall and size controlled nZVI. Therefore, in this work, the addition of a polymeric functionalizing agent for the stabilization of the nanoparticles for the control of agglomeration and size was implemented by the grafting of EG brushes on the surface of the particles. Accordingly, it is proposed the implementation of two stabilization mechanisms associated non-aqueous solvent use and the functionalizing agent and is expected that the two organic molecules, MeOH and EG, make interaction with nZVI, helping nZVI growth in controlled manner.

On the other hand, in view of that the magnetic attraction dominates the interaction energy in magnetic nanoparticles such as nZVI [59], the nanoparticles tend to rapidly agglomerate, limiting their mobility and stability in water, reducing their efficiency and application, mainly in the treatment of groundwater [26]. So that the increase in the dispersibility by materials functionalization and the size reduction that causes the decrease of the nZVI magnetic moment [25] will produce materials with a high nanosuspension.

This work presents a cost-effective synthesis method of size distribution <7.5% nZVI (1–9 nm) generated by non-aqueous chemical reduction method of ferric salts and functionalized with ethylene glycol at room temperature without inert conditions. Additionally the synthesis of zero-valent iron nanoparticles without coated agent (S-nZVI) was realized to compare the occurred effects in the different materials associated to the absence and presence of the functionalization, such as: the decrement in the particles diameter, control in size distribution, and the benefits of the grafted polymers in the colloidal stability and the reactivity of the nanomaterials.

The different stabilization mechanisms involved were analyzed by ultraviolet–visible (UV–Vis) absorption spectroscopy and Fourier transform infrared spectroscopy (FTIR). The structural characterization of the materials was carried out in terms of crystallinity, morphology, size distribution analysis, and colloidal stability. In addition, in Size distribution analysis were compare the materials obtained in this work by non-aqueous methodology (nZVI-EG_{non-aq} and S-nZVI_{non-aq}) and the surface modified nZVI generated by aqueous methodology (nZVI-EG_{aq}) presented in our precursory study, with the finality of demonstrate the advantages of the use of methanol as solvent. The reactivity of the materials was evaluated by the quantification of reactive iron content and the nitrate reduction capacity, similarly, in the reaction tests were evaluated the different materials nZVI-EG_{non-aq}, S-nZVI_{non-aq} and nZVI-EG_{aq}, to compare the different pollutant removal capabilities associated with particle size and functionalization.

3.2 MATERIALS AND METHODS

3.2.1 Reagents

Ferric chloride hexahydrate (FeCl₃·6H₂O) purchased from Fermont; sodium borohydride (NaBH₄), potassium nitrate (KNO₃), hydrochloric acid (HCl) and Methanol (CH₃OH) were obtained from Sigma-Aldrich. Ethylene glycol (EG) was purchased from Fluka. All the chemicals used in this study were of analytical grade without further purification.

3.2.2 nZVI synthesis

Nanoscale zero valent iron synthesis was performed by modifying the method proposed by [4] that consist of the chemical reduction of a ferric salt (FeCl₃) in methanol as solvent using NaBH₄ as reducing agent. Initially, a Fe³⁺

solution is prepared and 0.4 ml of EG is added and mixed for 5 minutes at 800 rpm without inert conditions at room temperature. Finally, 0.05 M of the reducing agent was added to the vessel and the nucleation process of the EG functionalized particles is initiated. S-nZVI was prepared under similar conditions without EG addition during the synthesis.

3.2.3 Physical characterization methods

In order to identify the mechanisms involved in the stabilization and functionalization, the coated sample was characterized with UV-Vis absorption spectroscopy using a S2000-UV-Vis spectrometer from OceanOptics Inc. and Fourier transform infrared spectroscopy (FTIR) using a Shimadzu IRAffinity-1. X-Ray data was obtained with a GBC-Difftch MMA diffractometer with filtered $\text{CuK}\alpha$ ($\lambda = 1.54 \text{ \AA}$) radiation. X-ray data analysis was obtained by subjecting the XRD data to Rietveld refinement [50] using the program MAUD in order to corroborate the presence of iron zero-valent ($\alpha\text{-Fe}$), iron oxide (Fe_xO_y) and to do phase quantification. The morphology was observed by transmission electron microscopy (TEM), carried out at 100 kV using a JEOL-1230. The average hydrodynamic size and Z-potential were measured with Nanosizer DLS. The sedimentation rate and colloidal stability of the produced nanoparticles with and without functionalization was tested by optical density at the 508 nm wavelength using a UV-Vis spectrophotometer (Cary 50, Agilent Technologies Inc., USA) based on the methodology reported by [26].

3.2.4 Reactivity analysis

Reactivity analysis of the different materials types was determined by the quantification of reactive iron contents by the hydrogen (H_2) gas measuring produced by acid digestion and the nitrates reduction [26,14]. The evaluation of the nitrate reducing capacity of the materials was carried out using the experimental methodology reported by [60].

3.3 RESULTS AND DISCUSSION

3.3.1 Functionalized nZVI prepared by non-aqueous reduction

3.3.1.1 Stabilization mechanisms

It has previously been reported that the functionalization mechanism of nanoparticles by the use of molecules with CHO terminal group is carried out through the interaction of several stabilization mechanisms. Firstly methanol molecule case, since methanol is an alcohol, it has an OH group, which has lone pairs of electrons available, therefore; it acts as a Lewis base able to react with Lewis acid (Fe^{3+}) by coordinating it. Wertz and Kruh (1969) reported the structures of the solute species of Fe (III) chloride - methanol in concentrated $\text{FeCl}_3\text{-MEOH}$ solutions, analyzing the dissociation of the $\text{FeCl}_3\cdot 6\text{H}_2\text{O}$ salt in non-aqueous solvent, establishing a solute model to explain the solvation of iron ions in methanol,

which is carried out by octahedral coordination of Fe^{3+} with four iron-oxygen bonds and two chlorine-iron bonds $[\text{Fe}(\text{CH}_3\text{OH})_4\text{Cl}_2]^+$ [61]. The functionalization mechanism using EG as a stabilizing agent was previously reported in our previous publication (Claudio et al., 2017, submitted). The stabilization is performed by the interaction between partially positively charged surface of nZVI and the electron density of the last oxygen-contained orbitals in the COH group by the presence of Van der Waals forces [53] grafting the surface of the particle with polymer chains.

With respect to two mechanisms mentioned above, the use of non-aqueous solvent would have an important role on particle stabilization with surface polymer. It is possible to have a better grafting of the polymer brushes on the surface of the particle leading to a better stabilization and control of the size, by cause of the chemical properties of methanol because using a non-aqueous low polarity medium is possible reduce the electrostatic hydrogen-bridge-type interactions between the solvent and the polymer employed during the synthesis due to two facts; Firstly, exist a decrease in hydrogen bonding capacity in non-aqueous solvents in contrast to aqueous solvents associated with the reduction in bond length H Methanol (0.956Å) compared with water (1.97Å) [62] and the decrease in the number of H sites available to interact in the non-aqueous solvent lowered the electrostatic interaction and the bonds formation. Finally, a higher polarity in aqueous type solvents evidences a higher intensity tendency to form intermolecular bonds between the molecules of the solvent and the polymer. In fact, the phenomena mentioned above are reflected during the nanoparticles formation due to the retention or stabilization of the coated agent by hydrogen bonds in the solvent, thereby preventing the interaction with the surface of nZVI for its stabilization, generating particles with larger diameters and loss of a large percentage of the polymer in solution.

According to the information described above, and the facts revealed by UV-Spectra and FTIR in the following section, we propose that the obtaining of ultra-small and narrow size distribution functionalized nanoparticles by the non-aqueous method; Firstly the methanol generates a first mechanism of stabilization through the Fe^{3+} coordination due to the reaction with the methane CH_3OH molecules forming a relative stable complex $[\text{Fe}(\text{CH}_3\text{OH})_4]$ (Figure 9A-Rx. 1). Post-coordination the complex was reduced with sodium borohydride (NaBH_4) to form nuclei and the growth of the primary particles (Figure 9A-Rx. 2). However, a second mechanism of stabilization intervenes in the interaction of EG with the nanoparticles formed avoiding the agglomeration of these and making more efficient the synthesis of nZVI with a narrow size distribution (Figure 9A-Rx. 3).

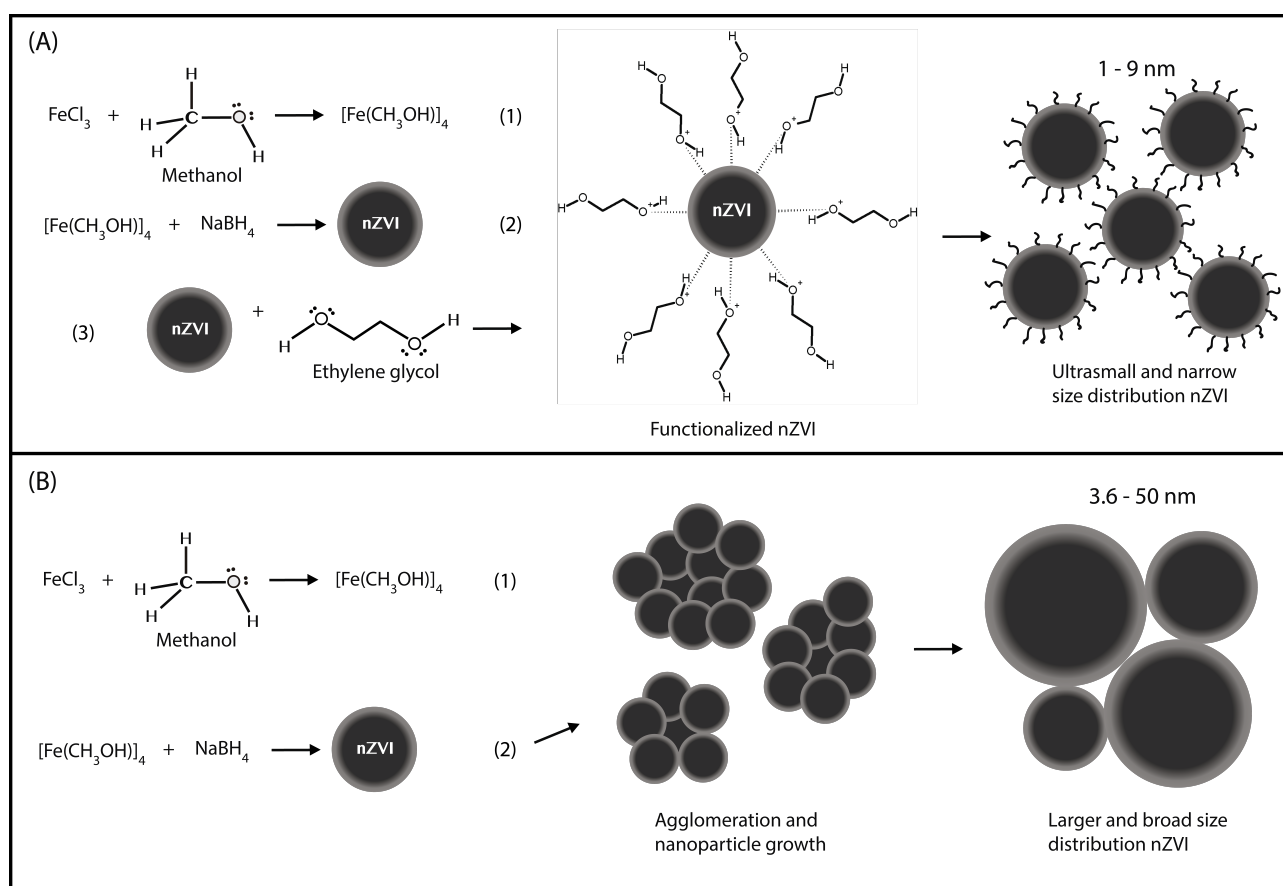


Figure 9. Schematic illustration showing: **(A)** Fe^{3+} coordination process, functionalization of nZVI-EG_{non-aq} and size-control. **(B)** Fe^{3+} coordination and uncontrolled grow of S-nZVI_{non-aq}.

3.3.1.2 Ultraviolet-visible (UV-Vis) absorption spectroscopy

UV-Vis absorption spectrum was analyzed in order to identify the interaction of CH_3OH molecules with Fe^{3+} during synthesis, comparing the cation characteristic spectrum in the aqueous and non-aqueous solvent at the same conditions (Figure 10A). Figure 10A display the absorption spectrum of FeCl_3 aqueous solution presents a band at 300 nm, which corresponds to the presence of Fe^{3+} ions. In contrast, the FeCl_3 non-aqueous solution presents the same band at 364 nm indicating a redshift band position that can be associated with Fe^{3+} coordination performed in the interaction between iron ions and CH_3OH molecules forming a relatively stable coordination compound $[\text{Fe}(\text{CH}_3\text{OH})_4]$. In fact [63] report the electronic absorption spectra for Iron (III) chloride in nonaqueous solvents and explain that the shift in band position in contrast to an aqueous medium is caused by the solvation of the salt in methanol generating the chemical species Cl^- and dichloro-iron (III) cation where the latter has an absorption peak at 366 nm.

In addition, absorption spectra were analyzed at different concentrations of water (0, 25, 50, 275 and 100%) with the purpose of analyzing the role of methanol in Fe^{3+} coordination related with band red shifted. In Figure 10B is possible to observe that as the content of methanol increases, the band located at 300 nm is shifted to 364 nm.

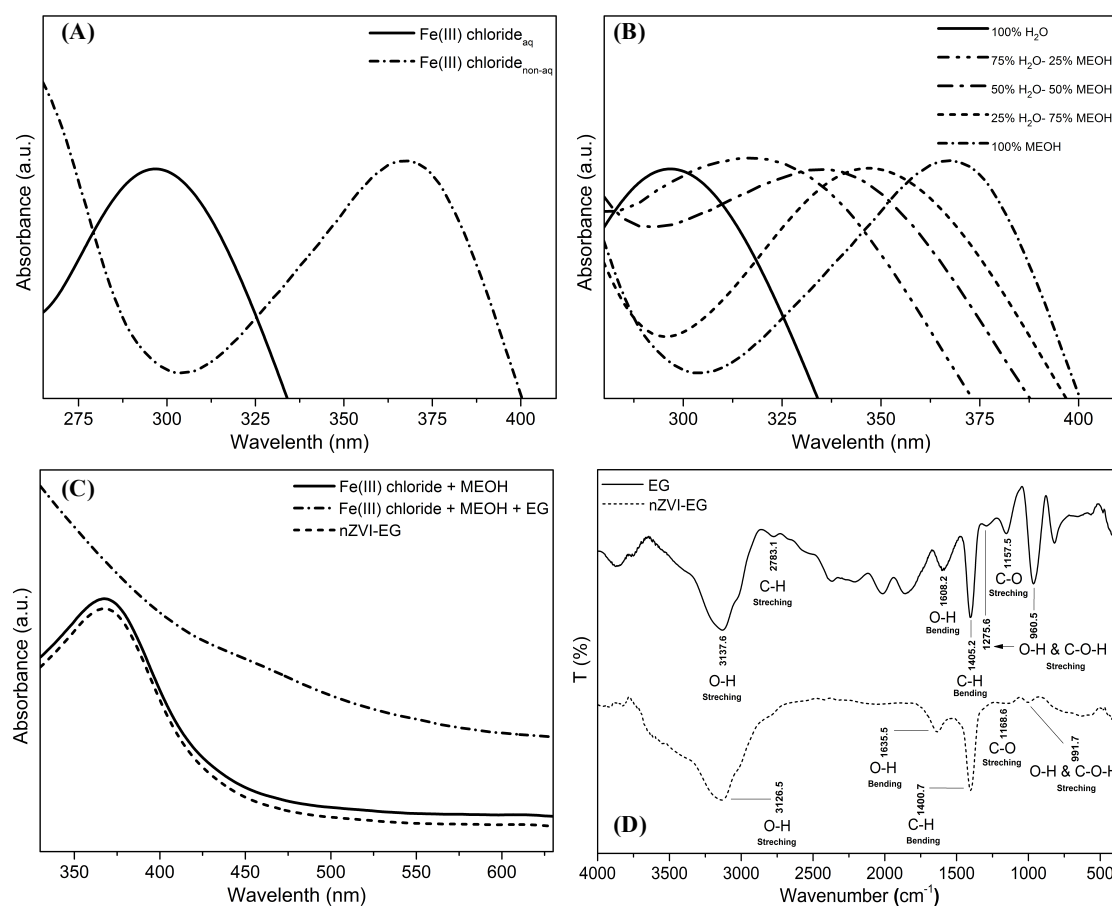


Figure 10. **A)** FeCl₃ aqueous and non-aqueous spectrum. **B)** UV-Vis absorption spectra of H₂O:MEOH; 100-0, 75-25, 50-50, 25-75 and 0-100%. **C)** [Fe(CH₃OH)₄], in the presence of EG and nZVI functionalized with EG spectra. **D)** FTIR spectrum of EG and nZVI-EG_{non-aq}.

Demonstrating that the red shift and the generation of [Fe(CH₃OH)₄] is directly proportional to the concentration of available methanol to react with Fe³⁺. It's in regards to stabilizing agent EG, when this is added to non-aqueous solution, no change can be observed in the absorption spectrum, so it is concluded that the first mechanism of stabilization is attributed solely to the interaction between CH₃OH and Fe³⁺. Subsequently, the addition of NaBH₄ was carrying out occurring the reduction of the complex formed and the nucleation process of nZVI. In the absorption spectrum belonging to Fe-Nps stabilized (nZVI-EG) there is a modification in the absorption band, which is completely different from the initial solutions having a maximum absorption peak at 250 nm (Figure 10C).

3.3.1.3 Fourier transform infrared spectroscopy (FTIR)

In order to corroborate the functionalization of nZVI and to identify the mechanism involved in the second step stabilization of the particles, EG molecule and EG nZVI stabilized was analyzed by Fourier transform infrared spectroscopy, comparing the vibrational frequencies associated with the functional groups present in the samples and examining the chemical bond changes occurred. Figure 10D and table 3 shows the FTIR analysis and band positions (cm⁻¹) corresponding to the asymmetric vibrational modes for EG and nZVI-EG. Infrared spectra of EG display a O-H

stretching vibrational mode presented at 3137.6 cm⁻¹, also at 2930 cm⁻¹ there is a sharp peak associated with C-H group asymmetric stretch deformation. At the wavenumber 1608.2 cm⁻¹ is located the peak corresponding to O-H flexural frequency vibrational of water molecules absorbed in the sample. Moreover, the peak at 1405.2 cm⁻¹ and **960.5** is associated with C-H molecule flexural strain. The wavenumber at 1275.6 and 960.5 cm⁻¹ could be assigned to the stretching of O-H and C-O-H molecules. Finally, the band position at 1157.5 cm⁻¹ is related with stretching of C-O group.

In case of nZVI-EG_{non-aq}, it is possible to see four principal bands at 3147.6, 3025.2 and 1394.6 cm⁻¹ assigned with O-H, C-H, O-H and C-O-H stretching vibrational mode corresponding, that the characteristic vibrational frequencies of EG. In addition the wave number at 994.3 cm⁻¹, which is associated with the deformation by stretching of the groups O-H and C-O-H in nZVI-EG that presents a noticeable decrease in the intensity of the band in contrast with EG (Figure 10D). This decrease in intensity is associated with the interaction of electron density of last orbital oxygen atoms present in the COH group of EG molecules and the positively charged surface of the zero-valent iron nanoparticles, weakening the COH bond due to the formation of a coordinate covalent bond O-Fe⁰ (Claudio et al., 2017, submitted) [52]. Through this effect, the grafted polymer on particles surfaces avoid their agglomeration by effects of excluded volume where the EG, chains in functionalized nanoparticles are located spatially at a short distance from another nZVI-EG occurring the repulsive interaction between EG, brushes. Because the polymer chains cannot occupy the same space, which decreases the number of conformations that the chain can take in contrast when they are at longer distances due to the superposition of the electronic clouds of the molecules [64]. In a similar way, it has been widely documented the steric repulsion between the nanoparticles in response to the increase of the local osmotic pressure where it is established that the overlap occurs of the polymer chains causing an increase in the concentration of the polymer in this region in comparison with the solvent generating this local pressure increment. Which in turn adding to the excluded volume effect decreases the freedom degrees of the system, which is thermodynamically harmful, thereby promoting the particles separation and the restoration of the energy balance in the system [65].

Table 3
Band positions (cm⁻¹) for EG and EG nZVI functionalized.

Compound	Band positions (cm ⁻¹)
EG	<u>960.5</u> , <u>1157.5</u> , 1275.6, <u>1405.2</u> , 1608.2, 2783.1, <u>3137.6</u>
nZVI-EG	<u>991.7</u> , 1168.6, <u>1400.7</u> , 1635.5, <u>3126.5</u>

Underlined wavenumbers represent the characteristic bands of EG while underlined and bold wavenumbers represent the wavenumber for O-H and C-O-H stretching vibrational mode. These results are typical for EG [53,52,66,67].

3.3.2 Size control using non-aqueous solvent with stabilization agent

3.3.2.1 Morphological characterization – TEM

The TEM images corresponding to the nZVI-EG_{non-aq} sample show a quasi-spherical morphology (Figure 11A). In addition, it is possible to see an arrangement of nZVI in clusters mainly caused by the magnetic dipole-dipole interactions of the particles, generating an arrangement of these in a magnetic cluster, this type of arrangement has previously been reported for nZVI with resembling sizes [24,33]. Similarly, the nanoparticles corresponding to the non-functionalized sample, present a quasi-spherical morphology (Figure 11B). Notwithstanding, contrasting with the functionalized sample, an arrangement of the particles is observed in a different way, occurring the alignment of these in chain structure, due to the same magnetic attraction effects to which the particles are subjected. However, this arrangement of structures is a behavior typically shown by nanomaterials of this type [4,60]. In addition, in our previous work, the formation of zero-valent iron nanochains, in the presence and absence of a functionalizing agent, EG, is described (Claudio et al., 2017, submitted), so it shows that the arrangement of the chain type structures is independent of the modification of the surface of the particles, indicating that this behavior is directly related to the size and particle distribution, which for the sample placed in clusters, nZVI-EG_{non-aq} is remarkably contrasting with the materials arranged in nanochain morphology.

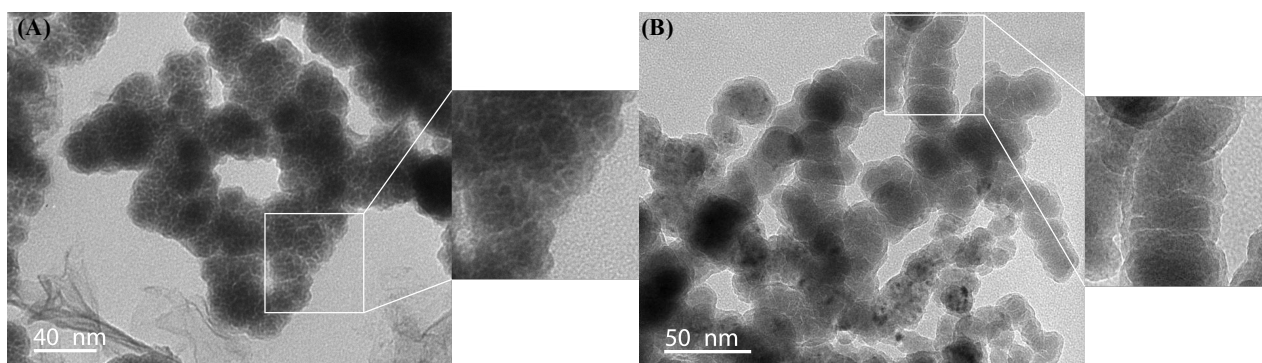


Figure 11. A-B) TEM photomicrography of nZVI-EG and S-nZVI correspondingly

3.3.2.2 Size distribution analysis

Statistical analysis of synthesized particles size distribution was carried out by the differential and cumulative distribution of the nZVI-EG_{non-aq}, SnZVI_{non-aq} and nZVI-EG_{aq} diameters in order to verify and compare the narrow size control and the predominance of low length in diameters of the functionalized and non-functionalized nanomaterials synthesized in non-aqueous solvent and demonstrate the advantage of using methanol as a solvent for particle size reduction. Over 472 measurements were made using different TEM microphotographs of the samples. The data corresponding to nZVI-EG_{aq} was adquired of our precursory study (Claudio et al., 2017, submitted). The statistical parameters obtained are showed in Table 4.

The differential distribution was adjusted using a non-linear lognormal distribution model to model the whole population behavior, which is widely used as reference model in nanomaterial size distribution analysis due to the low coefficients of variation calculated in comparison with different models used [68]. The differential particle size histogram displays a particle diameter range between 1-9 nm distributed in a normal manner indicating a positively biased asymmetrical geometry and a unimodal (single peak) distribution, but not monodisperse (all one size). The average particle size was calculated for this model with a value of 4.23 nm (Figure 12A).

The range of the particle diameter for the synthesized sample S-nZVI_{non-aq} at the first instance show a remarkable difference caused by the absence of the functionalizing agent, having a range of 3.6-50 nm, showed in a histogram also with a normal and asymmetrical geometry with a slight positive bias. The average diameter corresponding to this sample has a value of 23.68 nm, drastically increasing the particle size in compare with the first functionalized sample described (Figure 12B). The histogram corresponding to the sample synthesized in aqueous media in the presence of EG, presents a normal geometry unimodal but partially symmetrical, which denotes a contrast with the previously described histograms. The particle sizes are in the range 16.9-100.2 nm with an average size of 54.88 nm, which in the first instance marks a drastic increase compared to the samples obtained in non-aqueous solvent (Figure 12C).

The central dispersion trend of data distribution curve was evaluated using FWHM, for this work an absolute value of 2.65 nm was calculated in the range 2.66-5.47 nm, reflecting a low dispersion of data population (Figure 12A). For the non-functionalized sample the central dispersion presents a value such bigger of 33.17 nm in the range 9.91-43.08, demonstrating the widening of the size distribution according to the absence of the polymer (Figure 12B). Finally, for the case of nZVI-EG_{aq} the value corresponding to FWHM is 37.59 nm in the range 39.44-77.03 nm, which is a value close to that corresponding to S-nZVIN_{non-aq}, indicating at first instance a similar size distribution for both cases (Figure 12C). This is because, even though the diameter range of the particles is more extensive (16.9-100.2 nm), the size distribution is narrower, the frequency of a smaller range of diameters predominating. This could be possible due to the mechanism of functionalization and control in the size distribution by the presence of the polymer, EG, that modify the surface in these and producing steric repulsion effects (Claudio et al., submitted). In contrast, the sample S-nZVI_{non-aq} shows a much more uniform broad size distribution, which can be seen in the histogram, indicating similar frequencies in the different particle sizes. Proving that the particle stabilization mechanism by coordination of Fe³⁺ ions by the organic molecules of the solvent generates the reduction in particle size (3.6-50 nm). However, these particles do not maintain a control in the agglomeration and preservation of small diameters, due to the absence of a stabilizing agent that saturates the surface of the particles. Thereby obtaining a wide size distribution with significantly lower particle sizes with respect to the particles obtained by aqueous synthesis.

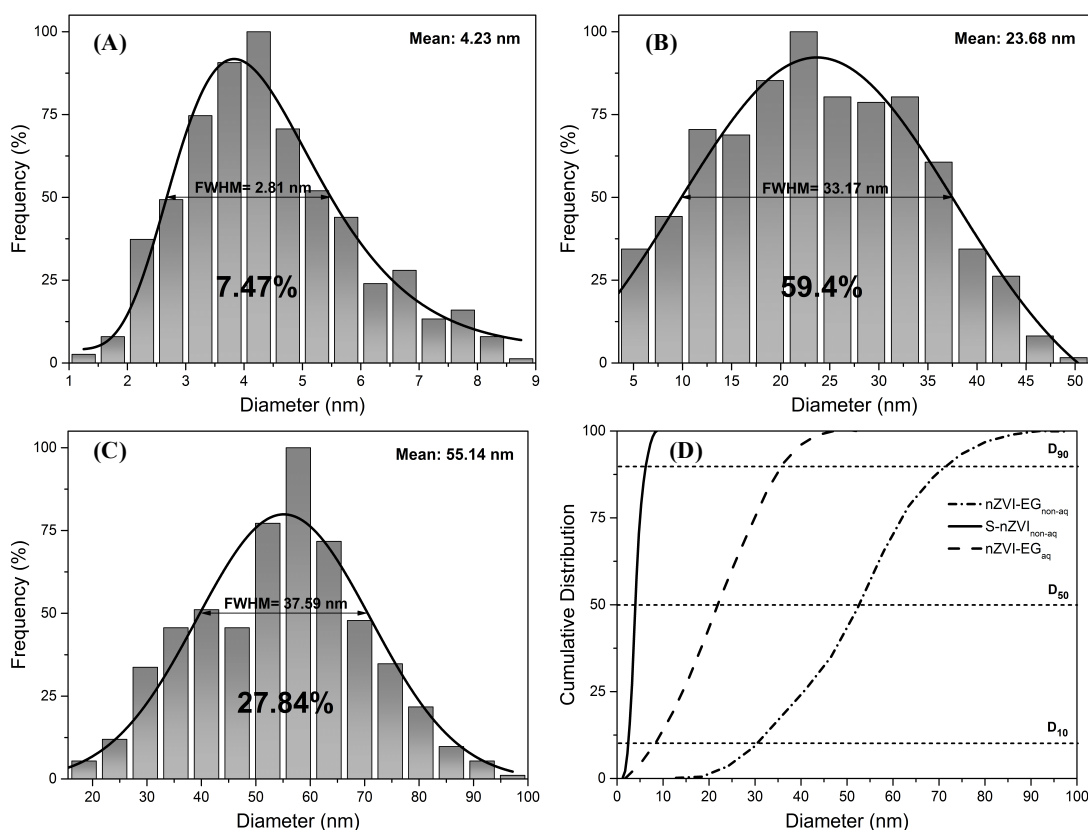


Figure 12. Differential and cumulative size distribution of **A)** nZVI-EG_{non-aq}, **B)** S-nZVI_{non-aq} and **C)** nZVI-EG_{aq}. **D)** Cumulative size distribution of the samples.

Another technique to measure data propagation with respect to arithmetic mean is the coefficient of variation (CV) or relative standard deviation (DSR), which is independent of the units and is expressed in % giving a better visualization and understanding of the propagation of the independent variable with respect to the average value. The value obtained associated to nZVI-EG_{non-aq} for this analysis was <7.5% (1-9 nm) indicating a narrow size distribution for materials of this type and quite bigger value of <60% (3.6-50 nm) corresponding to the broad size distribution of S-nZVI_{non-aq} (Figure 12A-B). The CV value obtained for nZVI-EG_{aq} gives a value of 27.84% (16.9-100.2 nm), which is close to half of the value corresponding to S-nZVI_{non-aq} (Figure 12C), indicating better the great difference in dispersion of the set of diameters analyzed. By obtaining this parameter it is possible to appreciate a marked difference between the various size distributions, which corroborates the information explained above between the size dispersions for the samples S-nZVI and nZVI-EG_{aq} and gives a better visualization of the predominance in the control of the narrow size distribution for the case nZVI-EG_{non-aq}.

The cumulative distribution of the sizes for nZVI-EG_{non-aq} sample shows that the distribution becomes narrower in sizes smaller than the median of the population (D_{50}) with a dispersion of 1.52 nm ($D_{50}-D_{10}$) indicating that 50% of the particles have diameters smaller than 3.90 nm. On the other hand it is possible to observe that 90% of the measured data

indicates particle sizes below 6.10 nm with which it is demonstrated; the domain of particles with diameters smaller than this length implying a good control of sizes during the synthesis and the little influence that the particles with dimensions larger than D_{90} in the sample (6.10-9 nm; Figure 12D). For the cumulative distribution of S-nZVI_{non-aq}, it is shown that 10% of the particle diameters are below 8.3 nm, however, these sizes grow importantly at D_{50} with a value of 22.01 and a dispersion of 13.7 nm. With respect to D_{90} the particle sizes below this percentage are less than 35.1 nm, which shows a significant increase with respect to the sample initially described (Figure 12D). In the cumulative distribution of nZVI-EG_{aq}, it is observed that only 10% of the diameters are smaller than 30.32 nm. Moreover, at the mean of the size distribution, we find sizes ≤ 52.66 nm and a dispersion of 22.34 nm. Therefore, at D_{90} , we find a value of 71.70 nm, which shows that only 10% of the diameters are in the range of 71.70-100.2 nm, showing a partially wide size distribution, by contrast with S-nZVI_{non-aq}. Nevertheless, this last sample shows that 90% of the diameters are smaller with respect to particles synthesized by aqueous phase methodology (Figure 12D).

The narrow size distribution of nZVI-EG_{non-aq} particles is demonstrated by approximation to zero of the relative measures of the differential distribution and otherwise the proximity to unity for the relative measures corresponding to the cumulative distribution. Even though between the two methods there is a large difference in nanoparticle size due to the second stabilization mechanism used, for S-nZVI_{non-aq}, it is possible to observe that the average size and 90% of the particles have sizes significantly smaller than nZVI-EG_{aq} using aqueous solvent, which demonstrates with this fact, the efficacy of methanol as a solvent in reducing and controlling size, however in the case of nZVI-EG_{non-aq} the control and reduction of the diameter is much greater than these reports which corroborates better the effectiveness of the use of both stabilization mechanism as a whole. In fact, specifically for the sample nZVI-EG_{aq} and the marked increase in size compare with the non-aqueous materials, two facts related to the type of solvent could be mentioned; Firstly, the advantages of the non-aqueous solvent use described above and second, the inhibition of the interaction among the methanol solvent and the polymer, EG, by means of bonds of type hydrogen bonding, retaining and stabilizing it. This creates a greater interaction of the polymer chain with the surface of the nanoparticles stabilizing them, avoiding their agglomeration with others for a better particles size control [69].

In view of the information described above, the size-controlled nZVI presented can be remarkably emphasized between different methodologies reported previously, which employ the use of aqueous, non-aqueous solvent and a mixture among them, due to various factors, such as; poor size control, broad size distribution, complex synthesis methodologies, and the use of inert conditions [4,33–35,52].

Table 4
Size distribution statistical parameters of ZVI materials in nm

Sample	Mean	CV (%)	FWHM	D ₁₀	D ₅₀	D ₉₀	D ₅₀ - D ₁₀	Span
nZVI-EG _{non-aq}	4.23	7.49	2.65	2.38	3.90	6.10	1.52	3.72
S-nZVI _{non-aq}	23.68	59.4	33.17	8.31	22.01	35.15	13.70	26.84
nZVI-EG _{aq}	54.88	27.84	37.59	30.32	52.66	71.70	22.34	41.38

3.3.2.3 Dynamic light scattering (DLS) and Zeta potential

Table 5 shows the hydrodynamic radius obtained by DLS measurement with obtained value of 6.5 nm for nZVI-EG_{non-aq} sample and 265.1 nm for the S-nZVI_{non-aq} without functionalization where the large diameter of the latter corresponds to the magnetic cluster generated by the rapid aggregation of the particles.

Moreover, the Z-potential for S-nZVI_{non-aq} and nZVI-EG_{non-aq} are calculated at +16.3 and -13.0 mV, respectively (Table 5). The difference in polarity of Z-potential associated with nZVI-EG_{non-aq} is due to the negatively charged groups present in EG that are not bound to the surface of the particle, which generates the attraction of positive countercharges, modifying the polarity of the hydrodynamic ratio. However, in spite of the different samples, they have opposite polarities, these are in similar ranges, which shows that there is an electrostatic repulsion between the nanoparticles, preventing their agglomeration, indicating that the forces of attraction between the particles are only of magnetic character. Therefore it is demonstrating with this information that the stable nanosuspension of nZVI-EG_{non-aq} and the small hydrodynamic conservation (6.5nm) is through the functionalization of the particles, due to the effects of saturated surface and steric stabilization [45].

Table 5
Dynamic light scattering (DLS) and Zeta potential of nZVI_{non-aq} samples

Sample	Particle size (nm)	Z potential (mV)
nZVI-EG _{non-aq}	6.5	+16.3
S-nZVI _{non-aq}	265.1	-13.0

3.3.2.4 Sedimentation analysis for nano-suspension stability examination

The sedimentation test of the materials was carried out in order to show the increase in the colloidal stability, the dispersibility and the reduction of the aggregation of the particles associated with the surface modification by the polymer brushes grafted and the reduction in the diameter of the particles attributed to the different stabilization

mechanisms used in this work. The curve was further analyzed using the one-phase decay equation, as described in our previous study [26].

$$I_t = I_0 e^{-t/\tau}$$

The curve associated with the nZVI-EG_{non-aq} sample shows an insignificant sedimentation rate at two hours, indicating that > 90% of the particles are kept in suspension during the sedimentation experiment. On the other hand, only <10% of particles were suspended in the case of S-nZVI_{non-aq} indicating very fast sedimentation (Figure 13). The characteristic time τ for the samples in the presence and absence of a functionalizing agent are calculated 1993 and 43.84 min, respectively, which is about 45 times difference. Associated with this information, Hwang et al., (2014) described that the increase in characteristic time is directly related to the reduction in hydrodynamic radius and by the decreasing stress in the size of the suspended particle, which explain the nZVI-EG_{non-aq} such great colloidal stability [26].

In fact that the conservation of >90% of the particles in suspension, can be related to size distribution analysis, where >90% of particles have sizes <6.10 nm, which possibly have a higher colloidal stability due to their size. However, these particles will be attracted by magnetic attraction and its eventual sedimentation. The saturation of the surface of the nanoparticles and the existence of steric repulsion in response to the functionalization of the material, increasing their dispersibility and delaying the rate of agglomeration and hindering the sedimentation of the particles [19,36] (Claudio et al., 2017, submitted).

Furthermore, it has been reported that a higher content of Fe(0) in the particles is associated a greater magnetic attraction force, which could generate the aggregation of the particles more quickly [59]. In view to this, the remarkable increase in the sedimentation rate for simple nZVI_{non-aq} in relation to the sample described above is related to the increment in diameter of the particles, because a magnetic moment of greater magnitude is associated with larger nZVI [25], benefiting the magnetic attraction between them. To give an illustration about this, the diameters corresponding to this sample are larger, meaning that the magnetic cores and core-shells made of magnetite are larger dimensions having greater magnetic force, therefore exist a greater interaction and attraction between the particles, generating with this, the formation of large fractal aggregates in chain-like structures, as is explained in DLS description, which will sediment with greater rapidity, due to this fact, even though 10% of the particles have diameters <8.31 nm, which possibly have a greater colloidal stability due to their size, these could easily be attracted by larger diameter particles cause the broad size distribution and subsequently to sediment.

The anti-aggregation capacity and the such high colloidal stability of nZVI-EG_{non-aq} can be compared with previous reports, where even with low Fe(0) content in the particles, low concentration of nZVI in the sedimentation tests and similar particle sizes, the nZVI is quickly agglomerated in solution leading to a precipitate and therefore is not shown a stability close to the values presented in this work [24,59]. Therefore it highlights the properties of our material and its applicability in environmental remediation, mainly for in situ subsurface remediation due to the possible high mobility of the nanomaterial in groundwater.

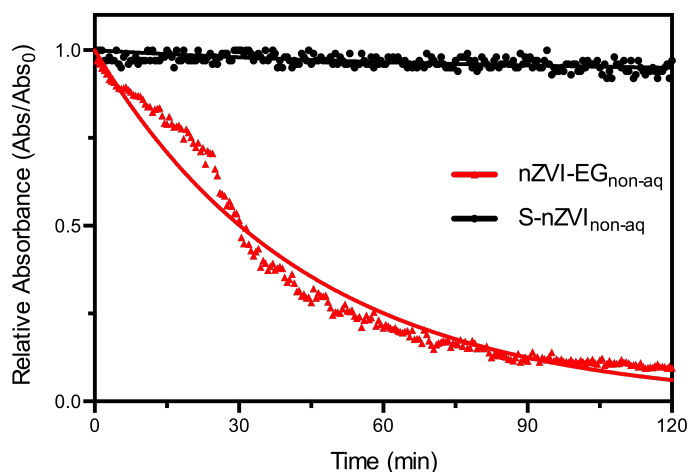


Figure 13. Sedimentation curves of nZVI and nZVI-EG

3.3.3 Effect of functionalization in reactivity of nZVI

3.3.3.1 X-Ray diffraction

The X-Ray diffractogram corresponding to nZVI-EG_{non-aq} shows the characteristic peak of the body-centered cubic (bcc) phase α -Fe located at 44.8° , that can be indexed as the (110) plane (JCPDS Card No. 79-0417). Diffraction patterns revealed a peak corresponding to the crystallographic phase magnetite (Fe_3O_4) at 35.4° indexed in the plane (311) (JCPDS 06-0696) that compounds the iron oxide core-shell that surrounds α -Fe. In a similar way the spectrum of S-nZVI_{non-aq} present with lower intensity the peak corresponding to α -Fe and magnetite peak with a greater intensity. Moreover, the diffracted peaks associated with the sample nZVI-EG_{aq}, represent the same crystallographic phases. However, with a marked increase in intensity and width, which is related to a better crystallinity of the material (Figure 6).

In the Rietveld refinement of the information of XRD is presents a greater percentage of the metal nucleus α -Fe and a smaller proportion magnetite for the case of functionalized samples with respect to the simple non-aqueous sample (Table 6). This conservation of the nucleus is due to the presence of the functionalizing agent, which prevents the additional oxidation of α -Fe (Claudio et al., 2017, submitted). Nevertheless, for non-aqueous samples, even if the

methanol can reduce this effect, will occur by the interaction of the material with the surrounding environment, owing to the increment in reactivity, caused by the particle size reduction. In light of this, is explained the higher iron core conservation of nZVI-EG_{aq}, due to the larger particle sizes. In the diffractogram the peaks corresponding to non-aqueous samples have a remarkable width, this widening of the peaks, this behavior for materials of this type has previously been presented where the synthesis of nZVI in water, ethanol and different proportions in the mixture of both are reported, demonstrating the stabilization and reduction of the particle size in the nanomaterials according to the increase of ethanol as solvent, which reflects a widening of the diffracted peaks for particles with smaller dimensions. This is associated with the decrease in the particle size with the spreading of the peaks in XRD because the size of the crystal is reduced increases the number of defects in the crystalline network in response to the smaller number of atoms available to assemble the crystallite and modify its behavior to one in an amorphous part with different network spacing, which is far from being an ideal crystal with an infinite number of flat crystals, obtaining with this a lower crystallinity and therefore a less intensity in the number of diffracted planes and the widening of peaks [70]. Despite to the widening of both spectra, a greater widening of the peaks is shown for the case of nZVI-EG, which can be related to the decrease of the diameter of the particle and the crystal, explaining the much greater crystallinity of nZVI-EG_{aq}, shown in the higher intensity and width of the peaks. . Notwithstanding, even with the widening of the diffracted peaks and the partial amorphous behavior, it is possible to see a better crystallinity for non-aqueous nanomaterials by contrast with amorphous nZVI with similar diameters reported before, owing to is possible detecting the peaks associated with the different crystallographic phases present in the samples [33,52]. Furthermore, the partially amorphous behavior of the spectrum makes difficult the calculation of the crystalline size to corroborate this.

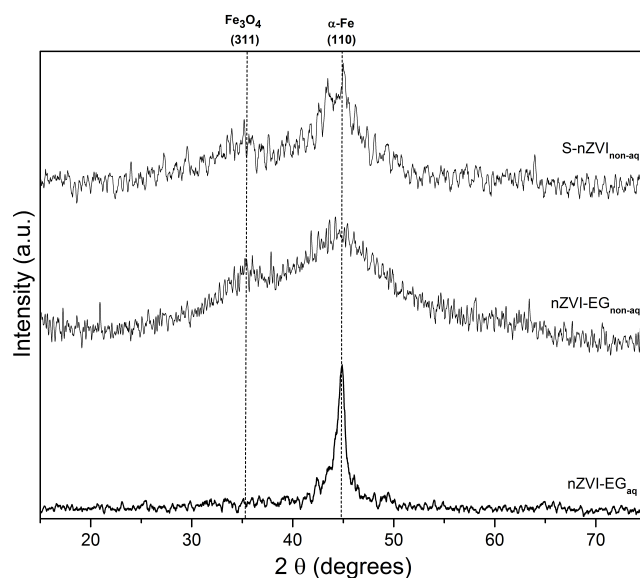


Figure 14. XRD pattern of S-nZVI and nZVI-EG.

Table 6
Rietveld refinement of a sample zero-valent iron nanoparticle.

Sample	α -Fe % in weight	Fe ₃ O ₄ % in weight
nZVI-EG _{non-aq}	86.42	13.58
S-nZVI _{non-aq}	81.02	18.98
nZVI-EG _{aq}	98.87	1.13

3.3.3.2 Reactive iron content

The amount of reactive iron in the synthesized samples indicates the degree of oxidation of the metal core, thereby demonstrating the stability of the particles during the synthesis, using methanol as the solvent without the need for inert conditions. The percentage of elemental iron for the sample without functionalization presented a value of 78.4% and 83.2% for nZVI-EG, both percentages confirm a high conservation of the reactive nucleus in the absence of inert conditions (Figure 15A). For this reason, taking as reference the reactive iron content obtained in the aqueous phase described in the precursory study, the percentages of Fe⁰ obtained in this work are similar, however, even though the use of methanol preserves the metal core, the loss of >15% of Fe⁰ in the materials is related to the high reactivity rate of the particles with the surrounding medium, because there is a notable difference in the compared materials in relation to size and particle size distribution, which is directly related to the increase of the surface area and the reactivity of these.

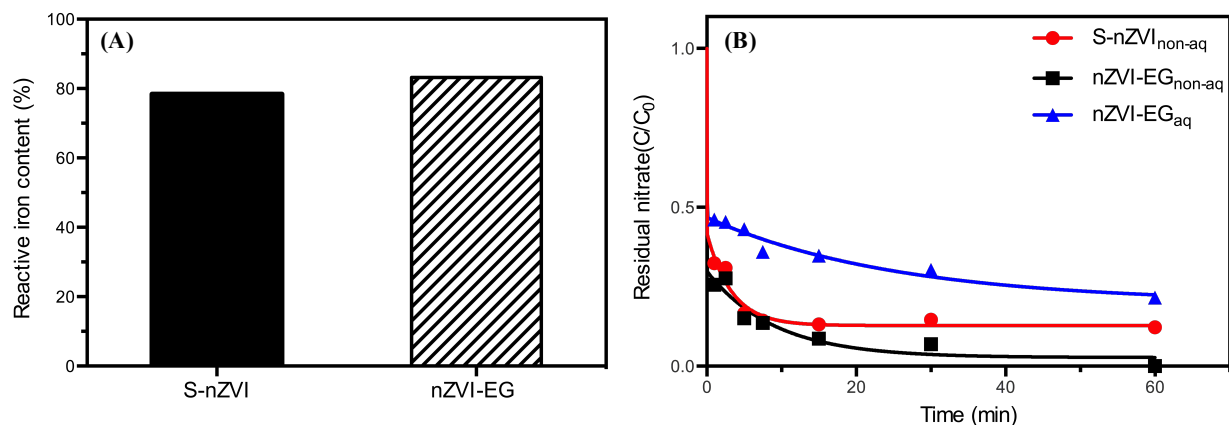


Figure 15. A) Reactive iron content of nZVI samples. B) Nitrate reduction by nZVI samples. (Conditions: 12.5 mg NO₃-N/L and 1000 mg Fe/L, pH 5, T=24±1°C).

3.3.3.3 Nitrate reduction

In this study, nitrate was selected as a model compound to confirm reducing reactivity of nZVI. It is well-known that nitrate is reduced to ammonia by the reaction with ZVI, therefore, we measured ammonia concentration to monitor nitrate reduction. Figure 15B presents nitrate reduction profile using **four** different nZVI we tested, explaining the effect of methanol and/or stabilizing agent, EG. The non-aqueous synthesized nZVI showed much higher reactivity in the beginning of reaction. For example, more than 70% of nitrate was removed in the first one minute of reaction, which

indicate almost instant reaction between nZVI and nitrate. On the other hand, the nZVI synthesized in aqueous condition could only reduce around 50% of nitrate in the same time, therefore, we could clearly see the effect of non-aqueous solvent, methanol, on nZVI reactivity. It is due to the decrement of particle size and size distribution using methanol.

Moreover, the nZVI-EG_{non-aq} showed better reactivity compared to S-nZVI_{non-aq} even though they were synthesized in methanol. Continuous nitrate reduction could be achieved in the case of nZVI-EG_{non-aq}, then all the nitrate was reduced in an hour. On the other hand, no more reduction was happened in S-nZVI_{non-aq} after 15 minutes of reaction. This is well corresponded with the sedimentation curve. The S-nZVI was aggregated together, especially between 20 – 30 minutes, therefore it forms large cluster not individual particles. The large cluster inhibit mass transfer as well as overall reaction, therefore, reaction got slow down after aggregation. Using functionalized nZVI in non-aqueous solvent can promise fast initial reaction due to the small size and narrow size distribution as well as long term reactivity due to low aggregation during reaction.

3.4 Conclusions

In this study, the effectiveness of methanol use as a non-aqueous solvent and ethylene glycol as stabilizing mechanisms for the synthesis of Ultra small, size-controlled nZVI without inert conditions was investigated. The first mechanism of stabilization occurs by the coordination of iron ions by MEOH molecules, which were further reduced to Fe⁰, subsequently occurs the second mechanism of stabilization by surface modification of the particles by EG brushes grafting, generating narrow Size distribution nZVI (<7.5%), where 90% of the particles have sizes <6.1 nm, which by the functionalization process, provides them a super high dispersibility in water, confirmed on stability testing by sedimentation analysis and DLS. Even in the absence of inert conditions in the synthesis, the XRD and iron reactive content analyzes showed a high conservation of the Fe (0) reactive nucleus. The reactivity tests in the reduction of nitrates, showed higher reactivity were observed with the contaminant in solution, associated with the such great colloidal stability, the ultrasmall diameters and narrow size distribution of the particles.

CHAPTER 4

4. CONCLUSIONS

In the present work, the synthesis of nanoscale zero-valent iron in aqueous and non-aqueous solvent was demonstrated, without the inert conditions, and using as a common factor the use of EG as a functionalizing agent, which plays a main role for each methodology. nZVI-EG_{aq}, showed that in the presence of the functionalization, it is air-stable, without showing a representative oxidation during the drying, and it was also increased the dispersibility of the nanoparticles in water. The protective effect of ethylene glycol was also revealed in its contaminant reduction capacity. It was possible to obtain high percentage of reactive iron and effective nitrate reduction, which indicates the effectiveness of nZVI functionalization by EG at preventing oxidation during the preparation of nZVI without inert conditions, intensifying the application and handling of the material in the environmental remediation field.

Corresponding to the case nZVI obtained in methanol, it was evidenced the reduction of size, by use of non-aqueous solvent, and by means of the addition of EG, it was possible to generate a second mechanism of stabilization for the obtaining of ultrasmall, size-controlled nanoparticles. Similarly by the presence of EG on the surface of the particles the dispersibility of the material was increased, which in conjunction with the low particles sizes generates such a high stability colloid. The different properties exhibited by the material, explain the high reduction capacity presented, therefore, can be defined as an effective tool in the treatment of water, which can be mainly applied in subsurface contamination remediation, where it is desired to have high mobility in the subsurface and short required time to degrade contaminants.

Moreover, for both materials, the reaction kinetics were not hindered by the addition of the organic functionalization agent EG, which also verifies the possibility of using EG in an effective surface modification method for nZVI.

REFERENCES

- [1] F. Fu, D.D. Dionysiou, H. Liu, The use of zero-valent iron for groundwater remediation and wastewater treatment: A review, *Journal of Hazardous Materials*. 267 (2014) 194–205. doi:10.1016/j.jhazmat.2013.12.062.
- [2] Wei-xian Zhang, Nanoscale iron particles for environmental remediation: An overview, *Journal of Nanoparticle Research*. 5 (2003) 323–332. doi:10.1023/A:1025520116015.
- [3] C.B. Wang, W.X. Zhang, Synthesizing nanoscale iron particles for rapid and complete dechlorination of TCE and PCBs, *Environmental Science and Technology*. 31 (1997) 2154–2156. doi:10.1021/es970039c.
- [4] Y.-P. Sun, X.Q. Li, J. Cao, W. Zhang, H.P. Wang, Characterization of zero-valent iron nanoparticles., *Advances in Colloid and Interface Science*. 120 (2006) 47–56. doi:10.1016/j.cis.2006.03.001.
- [5] Y. fan Su, C.Y. Hsu, Y. hsin Shih, Effects of various ions on the dechlorination kinetics of hexachlorobenzene by nanoscale zero-valent iron, *Chemosphere*. 88 (2012) 1346–1352. doi:10.1016/j.chemosphere.2012.05.036.
- [6] M.E. Morgada, I.K. Levy, V. Salomone, S.S. Farias, G. López, M.I. Litter, Arsenic (V) removal with nanoparticulate zerovalent iron: Effect of UV light and humic acids, *Catalysis Today*. 143 (2009) 261–268. doi:10.1016/j.cattod.2008.09.038.
- [7] S.S.R.M.D.H.R. Wijesekara, B.F.A. Basnayake, M. Vithanage, Organic-coated nanoparticulate zero valent iron for remediation of chemical oxygen demand (COD) and dissolved metals from tropical landfill leachate, *Environmental Science and Pollution Research*. 21 (2014) 7075–7087. doi:10.1007/s11356-014-2625-1.
- [8] H.S. Kim, J.Y. Ahn, K.Y. Hwang, I.L.K. Kim, H. Inseong, Atmospherically stable nanoscale zero-valent iron particles formed under controlled air contact: Characteristics and reactivity, *Environmental Science and Technology*. 44 (2010) 1760–1766. doi:10.1021/es902772r.
- [9] T. Tosco, M. Petrangeli Papini, C. Cruz Viggi, R. Sethi, Nanoscale zerovalent iron particles for groundwater remediation: A review, *Journal of Cleaner Production*. 77 (2014) 10–21. doi:10.1016/j.jclepro.2013.12.026.
- [10] T. Raychoudhury, T. Scheytt, Potential of Zerovalent iron nanoparticles for remediation of environmental organic contaminants in water: A review, *Water Science and Technology*. 68 (2013) 1425–1439. doi:10.2166/wst.2013.358.
- [11] M. Stefaniuk, P. Oleszczuk, Y.S. Ok, Review on nano zerovalent iron (nZVI): From synthesis to environmental applications, *Chemical Engineering Journal*. 287 (2016) 618–632. doi:10.1016/j.cej.2015.11.046.
- [12] W. Zhang, C.-B. Wang, H.-L. Lien, Treatment of chlorinated organic contaminants with nanoscale bimetallic particles, *Catalysis Today*. 40 (1998) 387–395. doi:10.1016/S0920-5861(98)00067-4.
- [13] D.W. Elliott, W.X. Zhang, Field assessment of nanoscale bimetallic particles for groundwater treatment, *Environmental Science and Technology*. 35 (2001) 4922–4926. doi:10.1021/es0108584.
- [14] Y. Liu, S.A. Majetich, R.D. Tilton, D.S. Sholl, G. V. Lowry, TCE dechlorination rates, pathways, and efficiency of nanoscale iron particles with different properties, *Environmental Science and Technology*. 39 (2005) 1338–1345. doi:10.1021/es049195r.
- [15] M.J. Alowitz, M.M. Scherer, Kinetics of nitrate, nitrite, and Cr(vi) reduction by iron metal, *Environmental Science and Technology*. 36 (2002) 299–306. doi:10.1021/es011000h.
- [16] A.M. Azzam, S.T. El-Wakeel, B.B. Mostafa, M.F. El-Shahat, Removal of Pb, Cd, Cu and Ni from aqueous solution using nano scale zero valent iron particles, *Journal of Environmental Chemical Engineering*. 4 (2016) 2196–2206. doi:10.1016/j.jece.2016.03.048.
- [17] C. Tiberg, J. Kumpiene, J.P. Gustafsson, A. Marsz, I. Persson, M. Mench, D.B. Kleja, Immobilization of Cu and As in two contaminated soils with zero-valent iron - Long-term performance and mechanisms, *Applied Geochemistry*. 67 (2016) 144–152. doi:10.1016/j.apgeochem.2016.02.009.
- [18] S. Li, W. Wang, F. Liang, W. Zhang, Heavy metal removal using nanoscale zero-valent iron (nZVI): Theory and application, *Journal of Hazardous Materials*. (2016) 1–9. doi:10.1016/j.jhazmat.2016.01.032.
- [19] R. Singh, V. Misra, R.P. Singh, Synthesis, characterization and role of zero-valent iron nanoparticle in removal of hexavalent chromium from chromium-spiked soil, *Journal of Nanoparticle Research*. 13 (2011) 4063–4073. doi:10.1007/s11051-011-0350-y.
- [20] M.N.A. Karlsson, K. Deppert, B.A. Wacaser, L.S. Karlsson, J.O. Malm, Size-controlled nanoparticles by thermal cracking of iron pentacarbonyl, *Applied Physics A: Materials Science and Processing*. 80 (2005) 1579–1583. doi:10.1007/s00339-004-2987-1.
- [21] H. Khalil, D. Mahajan, M. Rafailovich, M. Gelfer, K. Pandya, Synthesis of zerovalent nanophase metal particles stabilized with poly(ethylene glycol), *Langmuir*. 20 (2004) 6896–6903. doi:10.1021/la0497402.
- [22] J. Xu, A. Dozier, D. Bhattacharyya, Synthesis of nanoscale bimetallic particles in polyelectrolyte membrane matrix for reductive transformation of halogenated organic compounds, *Journal of Nanoparticle Research*. 7

(2005) 449–467. doi:10.1007/s11051-005-4273-3.

- [23] K.S. Suslick, M. Fang, T. Hyeon, Sonochemical synthesis of iron colloids, *Journal of the American Chemical Society*. 118 (1996) 11960–11961. doi:10.1021/ja961807n.
- [24] D.L. Huber, E.L. Venturini, J.E. Martin, P.P. Provencio, R.J. Patel, Synthesis of highly magnetic iron nanoparticles suitable for field structuring using a β -diketone surfactant, *Journal of Magnetism and Magnetic Materials*. 278 (2004) 311–316. doi:10.1016/j.jmmm.2003.12.1317.
- [25] D. Farrell, S.A. Majetich, J.P. Wilcoxon, Preparation and Characterization of Monodisperse Fe Nanoparticles, *The Journal of Physical Chemistry B*. 107 (2003) 11022–11030. doi:10.1021/jp0351831.
- [26] Y. Hwang, Y.C. Lee, P.D. Mines, Y.S. Huh, H.R. Andersen, Nanoscale zero-valent iron (nZVI) synthesis in a Mg-aminoclay solution exhibits increased stability and reactivity for reductive decontamination, *Applied Catalysis B: Environmental*. 147 (2014) 748–755. doi:10.1016/j.apcatb.2013.10.017.
- [27] S.R. Kanel, B. Manning, L. Charlet, H. Choi, Removal of arsenic(III) from groundwater by nanoscale zero-valent iron, *Environmental Science and Technology*. 39 (2005) 1291–1298. doi:10.1021/es048991u.
- [28] A. Liu, J. Liu, J. Han, W.X. Zhang, Evolution of nanoscale zero-valent iron (nZVI) in water: Microscopic and spectroscopic evidence on the formation of nano- and micro-structured iron oxides, *Journal of Hazardous Materials*. 322 (2017) 129–135. doi:10.1016/j.jhazmat.2015.12.070.
- [29] A. Liu, J. Liu, B. Pan, W. Zhang, Formation of lepidocrocite (γ -FeOOH) from oxidation of nanoscale zero-valent iron (nZVI) in oxygenated water, *RSC Adv*. 4 (2014) 57377–57382. doi:10.1039/C4RA08988J.
- [30] A. Liu, W. Zhang, Fine structural features of nanoscale zero-valent iron characterized by spherical aberration corrected scanning transmission ... iron characterized by spherical aberration, *The Analyst*. 139 (2014) 4512–4518. doi:10.1039/C4AN00679H.
- [31] Y. Sun, X. Li, W. Zhang, H.P. Wang, A method for the preparation of stable dispersion of zero-valent iron nanoparticles, 308 (2007) 60–66. doi:10.1016/j.colsurfa.2007.05.029.
- [32] F. He, D. Zhao, Preparation and Characterization of a New Class of Starch-Stabilized Bimetallic Nanoparticles for Degradation of Chlorinated Hydrocarbons in Water, 39 (2005) 3314–3320.
- [33] Q. Wang, S. Snyder, J. Kim, H. Choi, Aqueous ethanol modified nanoscale zerovalent iron in Bromate reduction: Synthesis, characterization, and reactivity, *Environmental Science and Technology*. 43 (2009) 3292–3299. doi:10.1021/es803540b.
- [34] G. V. Lowry, K.M. Johnson, Congener-specific dechlorination of dissolved PCBs by microscale and nanoscale zerovalent iron in a water/methanol solution, *Environmental Science and Technology*. 38 (2004) 5208–5216. doi:10.1021/es049835q.
- [35] S. Ambika, I.M. Nambi, Optimized synthesis of methanol-assisted nZVI for assessing reactivity by systematic chemical speciation approach at neutral and alkaline conditions, *Journal of Water Process Engineering*. 13 (2016) 107–116. doi:10.1016/j.jwpe.2016.08.011.
- [36] D. Pan, X. Ji, L. An, Y. Lu, Observation of nucleation and growth of CdS nanocrystals in a two-phase system, *Chemistry of Materials*. 20 (2008) 3560–3566. doi:10.1021/cm7023718.
- [37] M. Yue, Y. Li, Y. Hou, W. Cao, J. Zhu, J. Han, Z. Lu, Hydrogen Bonding Stabilized Self-Assembly of Inorganic Nanoparticles: Mechanism and Collective Properties, (2015).
- [38] R.A. Sperling, W.J. Parak, Surface modification, functionalization and bioconjugation of colloidal inorganic nanoparticles, *Philosophical Transactions of the Royal Society A: Mathematical, Physical and Engineering Sciences*. 368 (2010) 1333–1383. doi:10.1098/rsta.2009.0273.
- [39] Z. Qian, S.P. Hastings, C. Li, B. Edward, C.K. McGinn, N. Engheta, Z. Fakhraai, S.J. Park, Raspberry-like metamolecules exhibiting strong magnetic resonances, *ACS Nano*. 9 (2015) 1263–1270. doi:10.1021/nn5050678.
- [40] S.S. Shankar, A. Rai, A. Ahmad, M. Sastry, Rapid synthesis of Au, Ag, and bimetallic Au core-Ag shell nanoparticles using Neem (*Azadirachta indica*) leaf broth, *Journal of Colloid and Interface Science*. 275 (2004) 496–502. doi:10.1016/j.jcis.2004.03.003.
- [41] S.M. Alia, K. Jensen, C. Contreras, F. Garzon, B. Pivovar, Y. Yan, Platinum coated copper nanowires and platinum nanotubes as oxygen reduction electrocatalysts, *ACS Catalysis*. 3 (2013) 358–362. doi:10.1021/cs300664g.
- [42] D.T. Phan, A.S.M.I. Uddin, G.S. Chung, A large detectable-range, high-response and fast-response resistivity hydrogen sensor based on Pt/Pd core-shell hybrid with graphene, *Sensors and Actuators, B: Chemical*. 220 (2015) 962–967. doi:10.1016/j.snb.2015.06.029.
- [43] Y. Li, Z. Jin, T. Li, Z. Xiu, One-step synthesis and characterization of core-shell Fe@SiO₂ nanocomposite for

- Cr (VI) reduction, *Science of the Total Environment*. 421-422 (2012) 260–266. doi:10.1016/j.scitotenv.2012.01.010.
- [44] E. Harrison, J.R. Nicol, M. Macias-Montero, G.A. Burke, J.A. Coulter, B.J. Meenan, D. Dixon, A comparison of gold nanoparticle surface co-functionalization approaches using Polyethylene Glycol (PEG) and the effect on stability, non-specific protein adsorption and internalization, *Materials Science and Engineering C*. 62 (2016) 710–718. doi:10.1016/j.msec.2016.02.003.
- [45] N. Lee, K. Choi, B. Uthuppu, M.H. Jakobsen, Y. Hwang, M.M. Broholm, W. Lee, Synthesis of iron nanoparticles with poly(1-vinylpyrrolidone-co-vinyl acetate) and its application to nitrate reduction, *Advances in Environmental Research*. 3 (2014) 107–116. doi:10.12989/aer.2014.3.2.107.
- [46] J.P. Rao, K.E. Geckeler, Polymer nanoparticles: Preparation techniques and size-control parameters, *Progress in Polymer Science (Oxford)*. 36 (2011) 887–913. doi:10.1016/j.progpolymsci.2011.01.001.
- [47] M. Antonietti, K. Landfester, Polyreactions in miniemulsions, *Progress in Polymer Science (Oxford)*. 27 (2002) 689–757. doi:10.1016/S0079-6700(01)00051-X.
- [48] A.H. Lu, E.L. Salabas, F. Schüth, Magnetic nanoparticles: Synthesis, protection, functionalization, and application, *Angewandte Chemie - International Edition*. 46 (2007) 1222–1244. doi:10.1002/anie.200602866.
- [49] D.L. Huber, Synthesis, properties, and applications of iron nanoparticles, *Small*. 1 (2005) 482–501. doi:10.1002/sml.200500006.
- [50] H.M. Rietveld, A profile refinement method for nuclear and magnetic structures, *Journal of Applied Crystallography*. 2 (1969) 65–71. doi:10.1107/S0021889869006558.
- [51] Y. Hwang, A. Salatas, P.D. Mines, M.H. Jakobsen, H.R. Andersen, Graduated characterization method using a multi-well microplate for reducing reactivity of nanoscale zero valent iron materials, *Applied Catalysis B: Environmental*. 181 (2016) 314–320. doi:10.1016/j.apcatb.2015.07.041.
- [52] M. Din, Ö. Metin, S. Özkar, Water soluble polymer stabilized iron(0) nanoclusters: A cost-effective and magnetically recoverable catalyst in hydrogen generation from the hydrolysis of sodium borohydride and ammonia borane, *Catalysis Today*. 183 (2012) 10–16. doi:10.1016/j.cattod.2011.05.007.
- [53] K. Shameli, M. Bin Ahmad, S.D. Jazayeri, S. Sedaghat, P. Shabanzadeh, H. Jahangirian, M. Mahdavi, Y. Abdollahi, Synthesis and characterization of polyethylene glycol mediated silver nanoparticles by the green method, *International Journal of Molecular Sciences*. 13 (2012) 6639–6650. doi:10.3390/ijms13066639.
- [54] F.M. Veronese, Peptide and protein PEGylation: a review of problems and solutions., *Biomaterials*. 22 (2001) 405–417. doi:10.1016/S0142-9612(00)00193-9.
- [55] K.T. Soto Hidalgo, E.O. Ortiz-Quiles, L.E. Betancourt, E. Larios, M. José-Yacaman, C.R. Cabrera, Photoelectrochemical Solar Cells Prepared From Nanoscale Zerovalent Iron Used for Aqueous Cd²⁺ Removal, *ACS Sustainable Chemistry & Engineering*. 4 (2016) 738–745. doi:10.1021/acssuschemeng.5b00601.
- [56] W. Yan, A.A. Herzing, C.J. Kiely, W.X. Zhang, Nanoscale zero-valent iron (nZVI): Aspects of the core-shell structure and reactions with inorganic species in water, *Journal of Contaminant Hydrology*. 118 (2010) 96–104. doi:10.1016/j.jconhyd.2010.09.003.
- [57] Y.-H. Hwang, D.-G. Kim, H.-S. Shin, Mechanism study of nitrate reduction by nano zero valent iron., *Journal of Hazardous Materials*. 185 (2011) 1513–21. doi:10.1016/j.jhazmat.2010.10.078.
- [58] J. Brillo, A.I. Pommrich, A. Meyer, Relation between self-diffusion and viscosity in dense liquids: New experimental results from electrostatic levitation, *Physical Review Letters*. 107 (2011) 1–4. doi:10.1103/PhysRevLett.107.165902.
- [59] T. Phenrat, N. Saleh, K. Sirk, R.D. Tilton, G. V. Lowry, Aggregation and sedimentation of aqueous nanoscale zerovalent iron dispersions, *Environmental Science and Technology*. 41 (2007) 284–290. doi:10.1021/es061349a.
- [60] Y.-H. Hwang, D.-G. Kim, H.-S. Shin, Effects of synthesis conditions on the characteristics and reactivity of nano scale zero valent iron, *Applied Catalysis B: Environmental*. 105 (2011) 144–150. doi:10.1016/j.apcatb.2011.04.005.
- [61] D.L. Wertz, R.F. Kruh, Structure of Iron (III) Chloride–Methanol Solutions, *The Journal of Chemical Physics*. 50 (1969) 4013–4018. doi:10.1063/1.1671661.
- [62] N. Zhang, Z. Shen, C. Chen, G. He, C. Hao, Effect of hydrogen bonding on self-diffusion in methanol/water liquid mixtures: A molecular dynamics simulation study, *Journal of Molecular Liquids*. 203 (2015) 90–97. doi:10.1016/j.molliq.2014.12.047.
- [63] R.S. Drago, D.M. Hart, R.L. Carlson, Spectrophotometric Studies of Iron (III) Chloride in Nonaqueous Solvents, *Journal of the American Chemical Society*. 87 (1965) 1900–1904.

- [64] M. Kurata, H. Yamakawa, Theory of Dilute Polymer Solution. I. Excluded Volume Effect*, *The Journal of Chemical Physics*. 2113 (1958) 785–791. doi:10.1063/1.1744272.
- [65] and A.G.G. R. López-Esparza, M. A. Balderas Altamirano, E. Pérez, Importance of molecular interactions in colloidal dispersions, *Advances in Condensed Matter Physics*. 2015 (2015). doi:10.1155/2015/683716.
- [66] S. Zheng, X. Li, Y. Zhang, Q. Xie, Y.S. Wong, W. Zheng, T. Chen, PEG-nanolized ultrasmall selenium nanoparticles overcome drug resistance in hepatocellular carcinoma HepG2 cells through induction of mitochondria dysfunction, *International Journal of Nanomedicine*. 7 (2012) 3939–3949. doi:10.2147/IJN.S30940.
- [67] W.-Y. Wang, J.-Y. Shi, J.-L. Wang, Y.-L. Li, N.-N. Gao, Z.-X. Liu, W.-T. Lian, Preparation and characterization of PEG-g-MWCNTs/PSf nano-hybrid membranes with hydrophilicity and antifouling properties, *RSC Adv*. 5 (2015) 84746–84753. doi:10.1039/C5RA16077D.
- [68] S.B. Rice, C. Chan, S.C. Brown, P. Eschbach, L. Han, D.S. Ensor, A.B. Stefaniak, J. Bonevich, A.E. Vladár, A.R. Hight Walker, J. Zheng, C. Starnes, A. Stromberg, J. Ye, E.A. Grulke, Particle size distributions by transmission electron microscopy: an interlaboratory comparison case study., *Metrologia*. 50 (2013) 663–678. doi:10.1088/0026-1394/50/6/663.
- [69] W. Tian, W. Mi, J. Tian, J. Jia, X. Liu, Z. Zhu, J. Dai, X. Wang, Comparative study on CdSe QDs synthesized from water and ethanol: Hydrogen bond induced particle agglomeration and enhancement on photoluminescence, *Analyst*. (2013) 1570–1580. doi:10.1039/c2an36658d.
- [70] S. Chen, Y. Zhang, W. Han, D. Wellburn, J. Liang, C. Liu, Synthesis and magnetic properties of Fe₂O₃–TiO₂ nano-composite particles using pulsed laser gas phase evaporation–liquid phase collecting method, *Applied Surface Science*. 283 (2013) 422–429. doi:10.1016/j.apsusc.2013.06.125.